

September 16, 2016

Dear Editor,

We have carefully revised our manuscript following the second round of reviews and feel that we have successfully addressed the referees' comments. We have further clarified unclear aspects of our mathematical model and approach. In Figure 1 we replaced the one-hour temperature hold experiment with a faster cooling rate experiment instead, as this is easier to understand and better illustrates the aspects of our model that we wish to highlight.

To address the issues raised regarding variability of particle surface area between droplets in the cold plate array, we have added shaded regions to Figures 5, 6 & 7 that reflect the predicted freezing temperature for droplets containing different particle surface areas based on the experimental droplet volume range obtained. We note that the possible spread in the droplet freezing curve does not account for the broadening of the freezing curves at low particle concentration, and thus an additional explanation such as the one we propose regarding external variability is required to account for the effects of particle concentration. We have also included additional figures in the response to the referees where the droplet freezing spectra for the individual runs from our cold plate are shown. These demonstrate that variability in droplet freezing temperature between replicate runs of the same particle sample and concentrations are within 1 K of each other.

We hope you find our revisions and responses to the referees to be complete and acceptable and look forward to having our manuscript accepted for publication in ACP. We thank you and both referees for the time you have all invested in the peer review of our work.

Best regards,
Ryan Sullivan

Response to Referee #1 – Gabor Vali

We thank Gabor Vali for continuing his insightful dialogue with us, and for taking the time to clearly articulate his understanding and critique of our analysis and framework. His comments have continued to help us to significantly improve the quality and clarity of our work. We have replied to the major and specific points raised below, and shown how we have revised the corresponding section of our manuscript. The referee's comments are in italics.

1 The problem of INP apportioning in drops (as I see it).

Freezing nucleation experiments with drops of uniform sizes and with equally distributed, known quantities of suspended material are evaluated in terms of some variants of Eq. (12) in Vali (2014) in many publications, including the one under discussion. The resulting $n_s(T)$ functions, or nucleus spectra, are considered good representations of the ice nucleating potential of the material examined. However, two additional factors have to be taken into account when the spectra are used in a predictive mode, i.e. applied to estimate freezing of drops of different sizes and with different concentrations of the material. These additional factors are, first, that the suspended material consists of particles of determinate sizes, and, second, that nucleating sites have finite dimensions and may require even larger areas around them to perform. Particle sizes can, in principle, be determined. Site areas are not well known.

One issue arising from the factors just described is how nucleating sites are apportioned among drops when the average number of sites per drop is low and an unequal distribution of the number of sites can be expected. Such low numbers are bound to be the reality for sites active at higher temperatures, the scarcity gradually increasing with increasing temperatures. This is a fairly straightforward problem to address via the Poisson distribution, either in terms of total surface area expected per drop, or in terms of the number of INPs (Vali, 1971). Particle sizes and the average number of particles per drop need to be known if surface rather than number of INPs is used. It is prudent that the $n_s(T)$ or $K(T)$ spectra be applied only over the range for which it has been derived from experiment, i. e. not to extrapolate algebraic representations of the spectrum.

The possibility that particle sizes become too small to contain nucleating sites is more difficult problem. It can probably be addressed with experiments using particles of different sizes, but, as far as I know, such experiments have not been possible so far with particles small enough for the limit to be reached. Theoretical estimates of the dimensions required for nucleating sites of different degrees of activity are not reliable, though models of molecular clustering are beginning to provide some indications.

2 The approach of Beydoun et al. and its critique

The paper develops a scheme for dealing with the issue of small average particle surface area per drop. Another problem, a saturation effect, is also considered but that is not a real issue, in my opinion.

Whether the approach of this paper is better (more practical, more intuitive etc.) than the one sketched in the rest part of this comment can be judged by examining the details of the method proposed in this paper. This view already incorporates the judgment that the proposed theory does not present new insights but is a procedure to improve data interpretation. Thus, the origin of the assessment of ice nucleating ability comes from experiment, not theory.

Yes, we agree. Results derived from cold plate freezing spectra with decreasing particle concentration have contributed to the formulation of a critical area hypothesis. Therefore, experimental observations inspired our assessment and not theory. The g framework we present is an analysis method for interpreting cold plate droplet freezing spectra and deriving quantitative descriptions of ice nucleation properties of particles; it is not a development of a new theory regarding heterogeneous ice nucleation.

It may be useful to restate what I understand to be the tenets of this paper. The paper states that it is based on classical nucleation theory (CNT). As an aside, I note that this is a somewhat hollow claim, since the thermodynamic or kinetic aspects of that theory are not tested, nor do they impact the analyses done.

We have reworded the statement indicating that the work is based on CNT to say that the derivation of the framework starts with CNT. This we feel is a proper reflection of how the framework is developed since the derivation presented starts with CNT.

The text was revised as follows, on Page/Line 4/9-10:

“A new parameterization, starting from classical nucleation theory, is formulated in this paper.”

A rate equation analogous to Eq. 13 in Vali (2014) is used with contact angle as the measure of effectiveness. A normal distribution of contact angles, $g(\theta)$, is assumed, similarly to other publications. As a next step, in section 3.2 the distribution is limited by upper and lower limits θ_{c1} and θ_{c2} . The details of this process are, for me, the most obscure part of the paper. In principle, the resulting P_f probability function defines a spectrum of activity and serves the same purpose as the $K(T)$ or $n_s(T)$ spectra.

To describe the diminishing probability of finding nucleating sites in a drop, this paper introduces the concepts of external versus internal variability and the notion of a critical area. External variation arises when the particle surface area is reduced so that the full range of internal variation of INP effectiveness is not realized. The assumption of a normal distribution, which by definition is continuous to infinity at both ends, leads to the need for the critical area and critical contact angle range concepts. Below the critical area threshold, randomly sampled different g -distributions account for different experimental sets.

We agree that the resultant P_f probability serves the same function as $K(T)$ and $n_s(T)$ spectra, this is emphasized in our conclusion that one g distribution or an $n_s(T)$ function are sufficient to describe freezing behavior when enough ice nucleating material is present in a droplet on Page 34/5-21. While the g distribution is defined as a normal distribution and thus is continuous to infinity at both ends, the finite surface area restricts the contact angle range a particle will possess. The larger the surface area the higher the chance of possessing active sites with smaller contact angle values and thus the lower the values of the critical contact angles. We have added text in section 3.2 on page 12/19-22 to emphasize that the distribution does not need to be truncated to the range of the critical contact angles:

“It is important to emphasize that the critical contact angles are variable parameters and not a property of the ice nucleating species. Therefore, for the same g distribution the critical contact angles shift in the direction of decreasing activity (larger θ) for smaller surface areas and increasing activity (smaller θ) for larger surface areas.”

The fit shown in Fig. 1 by applying a distribution of contact angles (activity values), as opposed to using a single value of the contact angle, is the rst support given for the proposed scheme. Again, this has been shown already in other papers. Also, the it isn't really significant unless it is tested against empirical data for a number of different cooling rates. The emphasis of Section 3.1 of the paper is that a single particle is used for repeated tests, thus excluding external variability among drops. A number of other experiments of this kind have been described in Vali (2014, Section 3.1.2) and also discussed in Vali (2008) and Wright and Peters (2013). Reasons for the spread of observed freezing temperatures are interpreted there, and supported by other publications, as a combination of time-dependence (stochasticity) and possible alterations of the particle surface. The prediction in Fig. 1 for a 1-h holding time is not supported by evidence, in fact it is contrary to data reviewed in Vali (2014, Section 3.2.2) and Vali and Snider (2015, Section 2.3).

We realized that the prediction of the 1 hour folding time freezing probability can be replaced with a prediction with a different cooling rate. This makes the point being made in section 3.1 more

comprehensible as freezing curves of the same type are now being compared. The newly added predicted result of a shift in the median freezing temperature of 2 K for a reduction in the cooling rate from 10 K/min to 1 K/min is consistent with some studies on cooling rate dependence such as Herbert et al. (2014). However, we have also strengthened our emphasis that the aim of this exercise is merely to highlight how modeling the ice nucleating activity can have an impact on what parameters (e.g. time in this case) become more or less important. The text has been revised on Page 9/13-30 and Page 10/1-12:

“Two droplet freezing probability fits (dotted lines) are also plotted in Fig. 1 using the single and multiple θ fits but with a larger cooling rate of 10 K/min. One fit uses the same g distribution used previously, while the additional single θ fit is approximated as a normal distribution with a near zero standard deviation, similar to a Delta Dirac function. The resultant freezing probabilities are then computed and plotted for every T using Eq. (9). It can be seen that the g fit retains much stronger cooling rate dependence, with the freezing probability curve shifting about 2 K colder and the single θ curve shifting just 0.5 K colder for the faster 10 K/min cooling rate. The 2 K prediction presented here is still smaller than the one retrieved experimentally by Fornea et al. (2009) for varying the cooling rate from 1 K/min to 10 K/min, which was measured to be 3.6 K. However it is unclear which of the samples presented in their work corresponds to this change in median freezing temperature as it is only mentioned as an average decrease in temperature for all of the different samples tested.

This numerical exercise shows that wider g distributions theoretically yield stronger time dependence due to the partial offset of the strong temperature dependence that the nucleation rate in Eq. (2) exhibits. The result emphasizes that how the active sites are modeled has consequences on what physical parameters (e.g. time, temperature, cooling rate) can influence the freezing outcome and predicted droplet freezing temperature spectrum (Broadley et al., 2012) and that model parameters need to be tested under different environmental conditions (e.g. different cooling rates) to properly test their validity. In Fig. 1 a wider g distribution resulted in a higher sensitivity to cooling rate, which resulted in a shift of the freezing curve to lower temperatures as the system was cooled at a faster rate. This significant change in the freezing probability’s sensitivity to temperature is the cause of the more gradual rise in the freezing probability for the system when applying a non-Delta Dirac g distribution. This is effectively enhancing the stochastic element in the particle’s ice nucleation properties. The enhancement of the stochastic element brings about a more important role for time as shown in Fig. 1. The finding of this exercise is consistent with previously published work on time dependent freezing such as those reported by Barahona (2012), Wright and Petters (2013), and Herbert et al. (2014) amongst others.”

The main support for the critical area concept is seen in improved fits to fraction frozen curves for samples at low particle concentrations. When viewed in terms of $n_s(T)$ spectra, in Fig. 11, it is seen that gradually higher concentration values are derived as the particle loading is reduced. The upward shift for the Broadley et al. (2012) data set is almost inversely proportional to the increase in indicated surface area over a factor 30 change. For the CMU data set it is much less, about a factor 30 for a 500-fold decrease in loading. Each of these differences is smaller than the range of concentrations covered by data from any one of the samples, and the two data sets form a roughly consistent band covering eight orders of magnitude, also overlapping the data from Hiranuma et al. (2015). This broad consistency makes it seem somewhat secondary that within each set of experiments there is a trend toward higher n_s values with lower particle loading. Yet those trends are clear. While I find many faults with the critical area explanation of this paper, it does achieve a degree of success in rationalizing the effect. Looking at Fig. 11, it is less clear to me how the authors see a change only past a certain critical value. It should be noted that the scatter of data for any single experiment introduces considerable subjectivity in judging the quality of fitted functions and in the comparisons of different runs. Consequently, conclusions need to be read with caution.

We agree that the scatter of the data is an important caveat that we did not give proper attention to in our last version of the manuscript. Data from the CMU cold plate system has been compared to at least one other identical experiment to confirm reproducibility. More details on the experimental procedure and the reproducibility of the data presented have been added to the newly revised manuscript.

Text addressing the issues of surface area variability and the reproducibility of the data has been added on Page 23/7-30 and Page 24/1-11:

“One final thing to note is that the mathematical analysis presented here ignores the variability in total particle surface area present between droplets in each experiment. According to the range of droplet diameters mentioned in the Broadley et al. (2012) data of 10-20 μm surface area variability between the smallest and largest droplets in the experiment can be as high as a factor of 8. This assumes each droplet has the same particle concentration. While for the data presented from the CMU cold plate with droplet diameter varying from 500-700 μm , variability can be as high as a factor of 5. This assumes that the particle concentration is the same in each droplet, as they were produced from well-mixed particle suspensions in water. This surface area variability can be the source of an alternative explanation to the broadness of the freezing curves, whereby an analysis along the lines of what is presented in Alpert and Knopf (2016) can be applied.

The shaded regions of Figs. 5, 6a, and 7a show the predicted temperature range over which freezing of droplets occurs for the surface area variability associated with the diameter range of the considered experiments using \bar{g} (i.e. running Eq. (9) with different values for A). Figs. 5 and 7a show the predicted freezing variability for the highest and lowest mass concentrations while Fig. 6a only shows it for the highest concentration as the range predicted for the lowest concentration almost completely overlaps with the highest concentration. The prediction from surface area variability does contain the temperatures over which droplets freeze for the high concentration freezing curve but falls short of capturing the range for the low concentration-freezing curve. More importantly while the scatter in surface area between droplets can explain some of the broadness in the freezing curves, it is unable to explain why the curves become broader in the temperature range they span with decreasing surface area. Freezing temperature should respond linearly to surface area, if no other factors are changing (Eq. (9)). This observed trend is quite repeatable; according to Broadley et al. (2012) freezing temperatures were reproducible to within 1 K for their illite measurements, while for the CMU experiments for illite, MCC cellulose, and Snomax, the difference in freezing temperature spectra between at least two replicate experiments did not exceed 1 K. Therefore, if surface area scatter alone is proposed to explain the increasing variability of freezing temperatures with decreasing concentration/surface area, a cause for an increase in surface area scatter with decreasing concentration would have to be hypothesized. We recognize that such a surface area variability approach is also a viable one but the framework presented here presents an increase in the variability in ice nucleation activity with decreasing concentration/surface area as the means for describing the observed trends.”

We also show in the Figures below data for low concentration freezing curves of droplets containing cellulose (0.01 wt%) and Snomax (0.08 wt%) retrieved from multiple independent runs:

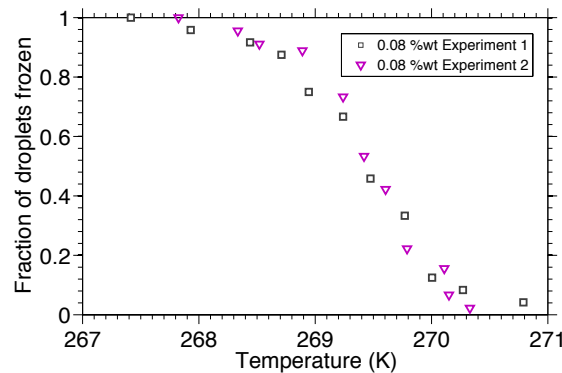


Figure A. Fraction of frozen droplets retrieved from two identical and independent cold plate experiments for droplets containing 0.08 % wt of Snomax.

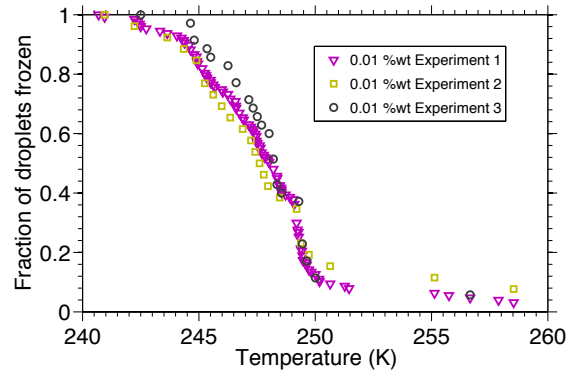


Figure B. Fraction of frozen droplets retrieved from two identical and independent cold plate experiments for droplets containing 0.08 % wt of MCC cellulose.

It can be seen that the values of the fraction of droplets frozen retrieved from multiple independent experiments fall within 1 K of each other.

The critical area notion introduced in this paper is similar to the idea expressed in Broadley et al. (2012) saying that "It appears that NX illite contains a rare particle/nucleation site type which dominates the freezing process when the overall surface area is greater than $2 \times 10^{-6} \text{ cm}^2$ per droplet." Interestingly this quote leaves it open that a different particle type is involved, as if the powder used in the tests contained a low proportion of some other material or other form of illite. In either case, it isn't easy to see a plausible reason for such critical value threshold phenomena in connection with ice nucleation. So, the arguments given in the paper (page 22, lines 10-20) about settling and coagulation of particles reducing the area effectively available for presenting nucleation sites do make some sense, though water would be still in contact with the particle surfaces even if aggregated into clumps and nucleation is not certain to be inhibited.

We agree, and point out that the effect of particle coagulation and settling on the $n_s(T)$ curves retrieved from cold plate experiments was focused on in a recent paper by Emersic et al. (2015) that we discuss in our manuscript.

Regarding the claimed saturation effect, I find the data less than convincing (considering potential errors) and the notion is counterintuitive, as I argued in the second comment I made on the first version of the paper (<http://www.atmos-chem-phys-discuss.net/acp-2015-1013/acp-2015-1013-RC2-supplement.pdf>). Can the critical area values derived in the paper be given any meaning in terms of interpretation, significance, comparison to other characteristics of the materials tested? If the activity of the INPs is a continuous function - with decreasing frequency toward higher temperatures - how can saturation (page 12 bottom) be achieved? A truncation of potential activity (at some $_$ value for this model) would be required for saturation to be realized. Do the authors have evidence to support that assumption? The data shown in Fig. 8 are not convincing for a 3 saturation effect since the lower portions of the fraction frozen curves move to higher temperatures as the particle loading is increased.

The saturation effect discussed in the paper is a physical effect whereby processes such as coagulation and settling inhibit increasing the available total particle surface area with increasing particle concentration at a high enough particle concentration. We think that this phenomenon occurring at a similar mass concentration in our experiments to the Broadley et al. experiments supports the claim especially since very different droplet volumes are used. The critical area hypothesis is different from the saturation effect and it does not imply that past a surface area threshold ice nucleating temperatures stop increasing with increasing surface area. As highlighted in a point above we do not truncate the distribution at the critical contact angles to carry out the critical area analysis. The hypothesis of the critical area is a means to mathematically describe the freezing trends observed as surface area is reduced, and at this stage we do not have direct physical evidence that ice nucleating species exhibit this behavior other than what is presented in the paper (i.e. uniform active site density functions are able to describe freezing behavior at high but not

low surface areas).

As for the high concentration data in Figure 8, we realize that the broadening in the freezing temperatures the droplets experience with added material makes the evidence less clear. But it should be said that the median freezing temperature remains the same with additional material so it seems as if there is a stronger variability in surface area past the saturation concentration. This could be because the hypothesized physical processes such as coagulation and settling are variable between droplets, though we admit that this is quite speculative. This is discussed on Page 22/28-31 and Page 23/1-6:

“Additionally, the high concentration freezing curves show a good degree of broadening in the temperature range over which freezing occurs. These three curves share a close 50% frozen fraction temperature (with the 0.5 wt% oddly exhibiting a slightly lower 50% frozen fraction temperature than the other two). One explanation that is consistent with the hypothesis of particle settling and coagulation is that it becomes less likely that the droplets contain similar amounts of suspended material when they are generated from such a concentrated suspension (Emersic et al., 2015). This results in larger discrepancies in available surface area between the droplets and therefore a broader temperature range over which the droplets are observed to freeze.”

3 Specific points.

Empirical data are used without any consideration of error ranges from limited sample sizes. This is specially serious at the upper end of the temperature range for each experimental run. It is conceivable that many of the discrepancies whose root cause is being examined in the paper arise from statistical uncertainties in the reported data. Having no objective measures of goodness of fit and weighting factors for data points from single runs leave most comparisons subjective. Multiple repetitions of the experiments would have been needed to increase the reliability of the data.

We have added text on the limitations presented by the potential scatter in surface area present in different droplets for each experiment. We acknowledge that it is a caveat of the analysis done. However all data presented and used for analysis was confirmed from at least two replicate runs of droplet arrays on our cold plate and the individual freezing curves observed are quite reproducible. Therefore, the trend observed below the critical area threshold is reliable. We added text to clarify this on Page 16/11-13:

“Around 50 0.1 μL droplets are then produced with a pipette from this solution. Each freezing experiment was repeated at least twice, with about 50 droplets per run, to confirm that the independently retrieved frozen fractions fell within 1 K of each other for each experiment..”

Other procedural errors solute effects, coagulation rates, settling, aging, contaminants, etc. also enter as samples of different particle loading are prepared. The authors themselves cite such processes as possible explanations for the high versus low particle loading observations.

Details about sample preparation whereby we attempted to reduce procedural errors have been added to the text on Page 15/29 and Page 15/1-10:

“We investigated a similar trend when freezing droplets containing commercial Snomax (York International), and MCC cellulose (Sigma-Aldrich) particles immersed in oil in our in-house cold plate system, described by Polen et al. (2016). The relevant system details are that particle-containing water droplets of approximately 500-700 μm in diameter are immersed in squalane oil, analogous to the method of Wright et al. (2013), and the droplets' freezing temperature is determined optically during a constant 1 K/min cooling cycle. A new sample solution is prepared of the material being tested before every experiment to avoid potential changes to the ice nucleation ability due to ageing. Ultra pure milli-Q water is used to minimize any background impurities that could provide a source of ice nucleants or solutes that would alter the freezing temperature of the water. Around 50 0.1 μL droplets are then produced with a pipette from this solution.”

Coagulation and settling are provided as possible reasons for the ceasing of an increase in the freezing temperature of the droplets at high concentrations. We argue that this saturation effect is a function of concentration and not surface area as both our illite experiments and the ones conducted by Broadley et al. (2012) observe this effect at similar concentrations despite different surface areas due to the differences in sample size. Text elaborating on this point is found on Page 22/19-31 and Page 23/1-6:

“Another important conclusion that can be drawn from this dataset is that high concentration data (0.25 wt%, 0.3 wt%, and 0.5 wt%) exhibited a similar plateauing in freezing temperatures despite additional amounts of illite. This is similar to the concentration range where Broadley et al. (2012) found a saturation effect when further increasing the concentration of illite (over 0.15 wt%). This supports the hypothesis that the high surface area regime for illite experiments is actually experiencing a particle mass concentration effect and not a total surface area effect. The fact that the concentration where this saturation effect is so similar while the droplet volumes and consequently the amount of illite present between the two systems is quite different points to a physical explanation such as particle settling or coagulation due to the very high occupancy of illite in the water volume. These physical processes could reduce the available particle surface area in the droplet for ice nucleation. Additionally, the high concentration freezing curves show a good degree of broadening in the temperature range over which freezing occurs. These three curves share a close 50% frozen fraction temperature (with the 0.5 wt% oddly exhibiting a slightly lower 50% frozen fraction temperature than the other two). One explanation that is consistent with the hypothesis of particle settling and coagulation is that it becomes less likely that the droplets contain similar amounts of suspended material when they are generated from such a concentrated suspension (Emersic et al., 2015). This results in larger discrepancies in available surface area between the droplets and therefore a broader temperature range over which the droplets are observed to freeze.”

The solution of Eq. (9) to yield a_{-t} for $g(\theta)$ needed some assumptions about $J(T, \theta)$ and that is not described in the paper. The exercise presented in Section 3.1 for a 1-h holding time is confusing, since it is unclear what the authors mean by "running Eq. (7) for the entire temperature range ..." (page 9, line 14).

Details about the assumptions needed to solve $J(T, \theta)$ have been added on Page 9/2-3:

“ $J(T, \theta)$ is evaluated using CNT parameters presented in Zobrist et al. (2007).”

As mentioned earlier in a response to a general comment, the exercise done in section 3.1 has been changed to compare freezing curves retrieved from two different constant cooling rates. This approach also allows for comparison with experimental data. The text has been changed on Page 9/13-30 and Page 10/1-12:

“Two droplet freezing probability fits (dotted lines) are also plotted in Fig. 1 using the single and multiple θ fits but with a larger cooling rate of 10 K/min. One fit uses the same g distribution used previously, while the additional single θ fit is approximated as a normal distribution with a near zero standard deviation, similar to a Delta Dirac function. The resultant freezing probabilities are then computed and plotted for every T using Eq. (9). It can be seen that the g fit retains much stronger cooling rate dependence, with the freezing probability curve shifting about 2 K colder and the single θ curve shifting just 0.5 K colder. The 2 K prediction presented here is still smaller than the one retrieved experimentally by Fornea et al. (2009) for varying the cooling rate from 1 K/min to 10 K/min, which was measured to be 3.6 K. However, it is unclear which of the samples presented in their work corresponds to this change in median freezing temperature as it is only mentioned as an average decrease in temperature for all of the different samples tested.

This numerical exercise shows that wider g distributions yield stronger time dependence due to the partial offset of the strong temperature dependence that the nucleation rate in Eq. (2) exhibits. The result emphasizes that how the active sites are modeled has consequences on what physical parameters (e.g. time, temperature, cooling rate) can influence the freezing outcome and observed droplet freezing temperature spectrum (Broadley et al., 2012). In Fig. 1 a wider g distribution resulted in a higher sensitivity to cooling rate, which resulted in a shift of the freezing curve to lower temperatures as the system was cooled at a faster rate. This significant change in the freezing probability's sensitivity to temperature is the cause of the

more gradual rise in the freezing probability for the system when applying a non-Delta Dirac g distribution. This is effectively enhancing the stochastic element in the particle's ice nucleation properties. The shallower response of freezing probability to decreasing temperature (deterministic freezing) creates a greater opportunity for time-dependent (stochastic freezing) to manifest, as a larger fraction of the droplets spend more time unfrozen. The enhancement of the stochastic element brings about a more important role for time as shown in Fig. 1. The finding of this exercise is consistent with previously published work on time dependent freezing such as those reported by Barahona (2012), Wright and Petters (2013), and (Herbert et al., 2014) amongst others."

3/18 More likely 2014 instead of 2008.

Yes, thank you. Vali (2014) provides the comprehensive survey of experimental results investigating time dependence. The reference has been changed.

3/20-27: There is a lot of vacillation in these sentences regarding the importance of time-dependence. More specific results are available in the literature. In line 21, "temperature fluctuations" is a poor choice of words for what the authors wish to say.

"Temperature fluctuations" has been changed to "variability in freezing temperature".

3/... Alpert and Knopf (2016) should be referenced and their approach contrasted with the one in this paper.

Alpert and Knopf (2016) has been added as a reference. Their method is mentioned and contrasted with ours on Page 23/15-17:

"This surface area variability can be the source of an alternative explanation to the broadness of the freezing curves, whereby an analysis along the lines of what is presented in Peter and Knopf (2016) can be applied."

And Page 25/19-24:

"Alpert and Knopf (2016) present a single component stochastic framework but successfully describe freezing behavior by considering surface area variability; more specifically defining a distribution of surface areas material in different droplets exhibits. A distribution of particle surface areas can provide a similar basis for variability in freezing temperatures between different particles as a distribution of ice nucleating activity."

4/16 What insights have been derived?

This sentence has been removed as the value of cold plate experiments run with varying concentrations is emphasized on Page 29/27-30 and 30/1-6:

"Cold plate experimental data potentially provides sufficient information to describe heterogeneous ice nucleation properties in cloud parcel and atmospheric models, however the analysis undertaken here suggests that retrieving one active site density parameterization (e.g. n_s) and applying it to all surface areas can result in misrepresenting the freezing behavior. When samples are investigated, probing a wide concentration range enables the determination of both general active site density functions (e.g. \bar{g}) as well as the behavior of the species' under study at more atmospherically relevant concentrations below the critical area threshold. Once this analysis is undertaken more comprehensive parameterizations can be retrieved as will be developed in the next section."

6/5: It is incorrect to reference Vali (2008) as a source for Eq. (3) using $J(T)$ in the exponent. The similar

equation in Vali (2008) is in terms of $n(T)$ which is time-independent. Eq. (3) implies that A and t have equivalent impacts, i.e. that a doubling of the surface area would produce the same result as a doubling of the time spent at some temperature T . This is not supported by evidence as the authors summarize on page 3. Anyway, the assumption of constant cooling rate eliminates the time variable going from Eq. (8) to (9).

Thank you for the clarification. We had previously made an error in referencing Vali (2008) as a source for Eq. (3). We now reference Pruppacher and Klett (1997) for that Equation.

7/5-6 Seems to contradict what is said later on (23/24-28).

We have reworded the referenced statement to emphasize that this is the first approach to use a continuous distribution to describe the freezing behavior of an individual particle in a droplet and not just the hypothetical distribution of active sites for an ice nucleating species. The text has been changed on Page 7/4-6:

“This is the first use of a continuum description of ice nucleating activity to describe the freezing behavior of an individual particle to our knowledge.”

8/8 ... There are several data sets presented in the referenced paper for volcanic ash. Which one was used here and why?

The freezing curve shown here is one of five samples of Mount St. Helens Ash tested in the immersion mode plotted in Fig. 7 in Fornea et al. (2009). It was chosen because it exhibited a larger spread in the freezing temperature from run to run. More details on the source and our choice of this data has been added to the text on Page 8/14-16:

“Five different particle samples of Mount St. Helens Ash were probed in the study; the one that exhibited the broadest range of freezing temperature was chosen for the examination conducted in this section.”

7/15-17: Is the meaning of "nucleating species" and "type" the same?

Yes. This sentence has been reworded to clarify this on Page 7/11-18:

“In this work the *internal* variability of an individual ice nucleating particle expresses the heterogeneity of its ice nucleating surface. A wider (larger σ) g distribution describes a greater particle internal variability of ice active surface site properties or contact angles present on that one particle. This is in contrast to the *external* variability of an ice nucleating species or type, which expresses how diverse a population of particles is in their ice nucleation activities. External variability accounts for differences in the g distributions of individual particles between particles of the same type (such as particles composed of the same mineral phases).”

11/22 What is meant by capturing "99.9% of the complete freezing probability"?

99.9% was intended to refer to the point at which the least square fit error assessed using Eq. (10) relative to Eq. (9) is below 0.01. The text has been clarified to reflect this on Page 11/24-25 and Page 12/1 as our previous description was not accurate:

“For the example studied in Fig. 3 (same system examined in Section 3.1), a value of $\theta_{c2} = 0.79$ rad results in a least square error of less than 0.01 for the freezing probability retrieved from Eq. (10) assessed against the freezing probability retrieved from Eq. (9).”

13/6 What is meant by "surface area density"?

The surface area density referred to here is the value of how much surface area a particle material is estimated to have relative to its mass. This has been clarified in the text and references are cited that use this parameter on Page 13/13-16:

"This estimate is retrieved from the weight percentage of the material in the water suspension and our best guess for a reliable surface area density, which is how much surface area a particle material possesses relative to its mass (Hiranuma et al., 2015a, 2015b)."

15/20-23 The brevity of this description of the origins of new data that were added in this version of the paper is welcome, but sample sizes (drop numbers), the origin of the illite sample and other essential details should have been given.

We agree that our last version of the manuscript lacked important details about the new experimental data we added to the revised version. We also reference our recent publication by Polen et al. (2016) that describes our cold plate system. New details have been added to the text on Page 15/29 and Page 16/1-13:

"We investigated a similar trend when freezing droplets containing commercial Snomax (York International), and MCC cellulose (Sigma-Aldrich) particles immersed in oil in our in-house cold plate system, described by Polen et al. (2016). The relevant system details are that particle-containing water droplets of approximately 500-700 μm in diameter are immersed in squalane oil, analogous to the method of Wright et al. (2013), and the droplets' freezing temperature is determined optically during a constant 1 K/min cooling cycle. A new sample solution is prepared of the material being tested before every experiment to avoid potential changes to the ice nucleation ability due to ageing. Ultrapure milli-Q water was used to minimize any background impurities that could provide a source of ice nucleants or solutes that would alter the freezing temperature of the water. Around 50 0.1 μL droplets were then produced with a pipette from this solution. Each freezing experiment was repeated at least twice, with about 50 droplets per run, to confirm that the independently retrieved frozen fractions fall within 1 K of each other for each experiment.."

And information on the origin of the illite sample can now be found on Page 22/6-11:

"We have conducted our own illite measurements on the same mineral sample used by Hiranuma et al. (2015) (Arginotec, NX nanopowder) to investigate this high concentration regime and further probe the applicability of \bar{g} to freezing curves above the identified critical area threshold. ."

20/15-19 How is it possible that the same trend in the right hand plots of Figs. 6 and 7 (shift to left for decreasing concentrations) leads to an downward order in Fig. 6b and the opposite in Fig 7b? Both samples are seen in the left hand plots to have decreasing activity with decreasing concentration, not just Snowmax, as claimed in the sentence later on this paragraph (20/26-27). Is there a data processing problem here?

The Snomax dataset exhibited an opposite trend in active site density, n_s , compared to illite and MCC cellulose whereby the reduction in concentration/surface area lead to a decrease in activity that was significantly lower than what would have been predicted by \bar{g} and n_s . This is not a data processing problem as we are confident in the change of ice nucleating activity that these experiments exhibit. Decreasing activity with decreasing concentration does not necessarily mean a decrease in active site density since the activity is determined by both the active site density and the surface area/amount of material present in the droplets. We also reference our recent Snomax study by Polen et al. (2016) where the freezing temperature is found to shift dramatically to lower temperatures with small decreases in particle concentration. This behavior matches what is known regarding the low abundance of the most efficient but fragile Type I ice nucleating proteins that freeze at -3 to -2 $^{\circ}\text{C}$, versus the more abundant and resilient but less efficient Type III proteins that freeze around -8 to -7 $^{\circ}\text{C}$. This peculiar behavior of the droplets containing Snomax is

mentioned on Page 16/26-31 and Page 17/1-9 while some explanation in the context of our framework is elaborated on in a response to a later comment:

“Unlike the illite dataset considered first, only 50% of the freezing behavior of the second highest concentration freezing curve is captured by a frozen fraction retrieved from \bar{g} (solid red line). Further lowering the concentration produces a similar trend previously observed for the droplets containing illite, with similar freezing onsets at higher temperatures but significant divergence at lower temperatures (purple and green points). The frozen fractions retrieved from \bar{g} for the 0.08 wt% and 0.07 wt% Snomax droplets (not plotted, as they almost overlap with the solid red line) do not capture any of the freezing behavior measured indicating a very sensitive dependence of active site density on surface area. A notable difference from the droplets containing illite is that there is significant weakening in ice nucleation ability as the concentration/surface area of Snomax is reduced. This behavior matches what is known regarding the low abundance of the most efficient but fragile Type I ice nucleating proteins that freeze at -3 to -2 °C, versus the more abundant and resilient but less efficient Type III proteins that freeze around -8 to -7 °C (Polen et al., 2016; Turner et al., 1990; Yankofsky et al., 1981).”

23/10-11 Perhaps you meant "... not to have a single ..."

We meant to say that the best fit Broadley et al. (2012) produced for their data was one where one single contact angle was assumed for each particle but that there was a distribution of contact angles for the particle population (as currently stated in the text). We emphasize in the text how for the low surface area freezing curves a model that assumed total external variability of active sites was better able to describe the data than one that assumed total internal variability.

25/25-28 The argument here seems backwards, as more active (low-contact angle) sites are less frequent and they can be assumed to be larger than less active ones.

While it may sound counterintuitive at first, the model predicts a more significant decline in the nucleating area contributing to the freezing of droplets at colder temperatures than the nucleating area contributing to early freezing. The nucleating area contributing to colder freezing is larger and statistically will experience a relatively larger decrease as the surface area of the system is reduced because there is a heavier reliance on active site frequency than active site strength compared to the nucleating area contributing to early freezing. This is how our framework explains the similar onset of freezing at higher temperatures as the surface area of material present in droplets is reduced but the divergence in the tail of the freezing spectra at lower temperatures (Figs. 5.6a, and 7a). We have reworded some of the text on Page 27/23-30 and Page 28/1-16 to help clarify this:

“Application of Eq. (11) to find $A_{nucleation}$ for illite systems 6a ($2.02 \times 10^{-6} \text{ cm}^2$) and 5a ($1.04 \times 10^{-6} \text{ cm}^2$) from Broadley et al. (2012) gives insight into how the nucleating area is influencing the shape of the freezing curves. System 6a is where the critical area cutoff was found to occur while 5a started to exhibit the behavior of a broader freezing curve with a similar onset of freezing but with a diverging tail, indicating it is below the critical surface area. In Fig. 6 the average cumulative ice nucleating area computed from Eq. (11) is plotted against the critical contact angle range for the two systems. In examining the cumulative nucleating areas two regions can be identified. The first region (0.95 rad to 1.15 rad) includes the stronger active sites that contribute to the earlier warmer regions of the freezing curves, while the second region (1.15 to 1.2) contributes to the tail and colder end of the freezing curves. The first region is broader in contact angle range but smaller in total nucleating area, therefore statistically there is a higher chance of particles of smaller area to draw these contact angles in the random sampling process. The second region is narrower in the critical contact angle range but occupies a larger fraction of the total nucleating area. Therefore, more draws are necessary to replicate the nucleating behavior of this region and thus there is a stronger drop off in the nucleating area represented by these less active contact angles as the surface of the particles is reduced.

This helps to explain why the onset of freezing for the two curves is so similar. The diverging tail can be attributed to the divergence of the nucleating areas at higher contact angles in the critical contact angle

range. The steeper rise of the average nucleating area of system 6a is due to its greater chance of possessing moderately strong active sites compared to system 5a due to the larger surface area present in 6a. This creates a larger spread in the freezing onset of droplets in system 5a after a few droplets initiated freezing in a similar manner to system 6a.”

26/13-15 How exactly does a "narrow range" explain the reverse trend in n_m for Snomax?

Compared to the cumulative nucleating area profile of illite, the Snomax nucleating area profile is much narrower in the critical contact angle range (Fig. 12). This leaves the chance of the nucleating area possessing two regions (one with stronger activity and less frequency and another with weak activity and more frequency) less likely. Without this, the smaller surface area Snomax particles become less likely to possess the ice nucleating activity of their higher surface area counterparts and a reduction in apparent active site density is realized. We emphasize that this is a mathematical finding and not a physical one. This is elaborated on in the text on Page 28/17-29 and Page 29/1-2:

“A similar nucleating area analysis was performed on the droplets containing Snomax and is shown in Fig. 12. The cumulative nucleating areas for the droplets with Snomax concentrations of 0.09 wt% and 0.08 wt% (red and green data in Fig. 8, respectively) are calculated and shown over the critical contact angle range with the same color scheme. Unlike the illite system, droplets containing Snomax exhibit a more straightforward trend in cumulative nucleating area vs. critical contact angle. The cumulative nucleating area is consistently smaller in the 0.08 wt% system compared to the 0.09 wt% experiment, indicating that as the particle surface area is reduced the strong nucleators are reduced uniformly over the critical contact angle range. This supports the idea that the range of active site activity is much smaller for this very ice active system. The consistent decline in nucleating area is attributable to the very narrow critical contact angle range the nucleating area covers (only 0.05 rad). We propose that this is what explains the decrease in n_m with decreasing concentration observed in Fig. 5. We stress however that this explanation is not physical and is merely a mathematical interpretation of the experimental trend being observed.”

Response to Referee #2

This is the review of the revised version of the manuscript now entitled “Effect of particle surface area on ice active site densities retrieved from droplet freezing spectra” by Beydoun et al.

This manuscript has greatly improved in clarity and data discussion. Inclusion of an additional co-author is justified. In general, I applaud the authors for the efforts responding to my comments, adding new experimental data, and make changes to the manuscript. Having said this, I am still not convinced that the ice nucleation data is sufficiently accurate to allow for such a study and its interpretation. The mathematical procedure is now much clearer, but I still have my doubts about its meaningfulness which will be substantiated below in more detail. Active sites may actually play a role in nucleation, however, I am not convinced that the presented exercise is sufficient to resolve this issue. Overall, I am not against publishing this work since it will hopefully stimulate more discussion in this direction. However, the authors should include the points and caveats mentioned below. Doing so will not change the novel analytical procedure, but may render some aspects more “relative” and maybe more “honest” what new science can be derived from these kinds of experiments and analysis.

We thank the referee for providing a second round of very well considered comments on our work. They have further clarified and strengthened the science we are presenting in our manuscript. We have addressed each point raised by the Referee below, and indicated how we have revised the text to address the points raised. The referee’s comments are in italics.

As I worked through this revision, I came across a study by Alpert and Knopf (2016) which made me also read Knopf and Alpert (2013) and Hartmann et al. (2016). Alpert and Knopf apply a stochastic freezing model and analyze surface area uncertainty for a variety of ice nucleation experiments including the cold stage experiment. They also include a discussion of the Hiranuma et al. (2015) intercomparison data. Hartmann et al. also point out the surface area uncertainty for CFDC experiments and also discuss the divergence in active site number densities as particle surface area varies.

The studies mentioned here by the referee are quite relevant and are now cited and discussed in the text. More on this follows in our responses to specific comments.

Beydoun et al. mention the stochastic nature of the freezing process several times in the manuscript. Alpert and Knopf show that results are statistically significant when a minimum numbers of freezing events are observed. They find that the Broadley et al. (2012) data using about 60 freezing events for a frozen fraction curve is not very statistically significant (Fornea et al.: 125 freezing events). In other words, the frozen fraction curves are prone to large uncertainties. They also show that in most experiments, surface area is likely uncertain by 1-2 orders of magnitude. For this manuscript, e.g., if actual surface area uncertainty were accounted for in the data of Fig. 5, all frozen fraction curves would be indistinguishable. When including the stochastic uncertainty and uncertainties in temperature, this would be even more indistinguishable within the error. For the newly presented experiments, the numbers of observed freezing events are not given. Also, the variation in droplet sizes, 200-300 nm and 500-600 nm, results in surface area uncertainties of more and less a factor 2-3. Again, this is an experimental issue and not necessarily one of the presented mathematical procedure.

In our newly revised version of the manuscript we have mentioned the caveats regarding surface

area uncertainties and discuss the resultant limitations. We discuss the reproducibility of the data analyzed and conclude that while surface area uncertainty can cover much of the scatter in freezing temperatures, it is unable to provide a standalone explanation for the trend of increasing range of freezing temperature with decreasing concentration. More details on this are discussed in our response to specific comments below.

As I read through these papers, I realized that Knopf and Alpert (2013) also investigated illite surface area dependent immersion freezing including below critical surface area data by Broadley et al. (2012). In their 2016 paper they are able to describe illite freezing data by Diehl et al. having large illite surface areas with the method published in 2013. What does this mean? Using nucleation rate coefficients instead of active site number density, seems to avoid the issue of particle surface area dependent active site number density? I think, at least these other methods/approaches must be briefly mentioned in the introduction and discussion sections.

For the illite data by Diehl et al. the surface areas (as pointed out by the referee) are large and therefore can be described with our \bar{g} approach for large surfaces (as shown in Fig. 8 of our paper), n_s (as shown in Fig. 11 of our paper), or an approach such as that presented by Alpert and Knopf (2016) whereby surface area variability in a single component stochastic model can account for the freezing variability observed. This other method/approach of Alpert and Knopf has been added to and discussed in our newly revised version of the manuscript as mentioned above and discussed further below.

Regarding the mathematical procedure and its much improved presentation: \bar{g} is determined for large surface areas. Interestingly, when you have a small number of draws ($n_{draws} < 25$, p. 18, l. 9), then the freezing curve will have a broader shape, but when $n_{draws} > 25$ the shape will be the same (i.e. the g^ distribution is the same as \bar{g}). What does this drawing from \bar{g} to make a discrete distribution g^* really tell us? For lower surface areas, the distribution has to become broader, resulting in a broader frozen fraction curve to represent the data. Instead of fitting a new distribution to that case of smaller surface area, by drawing, the authors use only certain pieces of \bar{g} and discard the remaining values of \bar{g} . Now this discrete distribution g^* (which are the pieces of the continuous \bar{g}), contains certain values which are “forced” to be chosen. For this reason, when sampling again randomly from g^* , the values of g^* will contribute much more compared to the original \bar{g} . In fact, doing so, g^* is an entirely new distribution analytically different to the original \bar{g} . This also means that g^* provides an increasing chance for larger and smaller contact angles to be used, compared to the \bar{g} . All that is happening is that a broader distribution is used that can better predict the data. In fact, the authors state this themselves: using $n_{draws} > 25$ and sampling from the resulting discrete g^* distribution is basically identical to sampling from the continuous \bar{g} distribution. This is obvious, since with a large numbers of draws, the majority of \bar{g} is resembled by g^* .*

So, if this is what mathematically is happening, this approach has no relation to active sites or internal and external mixtures. This is because this is only a mathematical procedure, i.e. find \bar{g} then change the distribution to find g^ . There is no surprise, when manipulating a distribution in above described way, that it becomes broader and better represents the data (which is likely not sufficiently constraint with respect to surface area and statistics as described above). I recommend being much more careful in the interpretation/statements of this mathematical procedure, in particular in the light if the Hartmann et al. and Alpert and Knopf*

studies are correct. I would defer making statements such as on p. 18, l. 23: “Thus it follows that there is a wider spread in the freezing curves for these droplets, as their freezing temperature is highly sensitive to the presence of moderately strong active sites. This expresses a greater diversity in external variability – the active site density possessed by individual particles from the same particle source.”

As a consequence of above said is, that all the apparent explanations such as stated "wider diversity in activity", "contain rare sites", "strong external variability", "strong nucleators at warm temperatures" are all non-testable statements. In summary, the reason that the frozen fraction curves are broader is because of the mathematical construct of the fitting including the number of draws. It is entirely due to this method of drawing to change the distribution from which frozen fractions are sampled. Lastly, all cumulative distributions ascend in a similar way due to the applied mathematical design and not because of some active sites. This seems not very “notable” to me (p. 18, l. 11).

The reviewer’s description of our numerical procedure is quite accurate. We should just emphasize that while drawing a contact angle is a random process in which any contact angle from $[0, \pi]$ can be chosen, the value of g^* at that random draw is assigned the value of \bar{g} . So contact angles with very small values at \bar{g} will still have small values at g^* carrying a negligible contribution to the new g^* distribution at that θ , and vice versa for the contact angles with large values at \bar{g} . So while g^* is a new distribution it still bears some resemblance to \bar{g} , as it is a random sample of it. The number of draws is intentionally reduced when trying to fit the broader freezing curves so that the modeled particle distributions express a greater degree of variability and can successfully describe the data. We have placed further emphasis on this procedure being a mathematical one and not having a basis in physical reality. However, we also emphasize that the freezing curve lines predicted using g^* are meant to represent the actual experimental freezing curves, where the broadening is observed. Therefore, it is important to understand that the broadening of the freezing curves is a real effect caused by reducing the particle concentration. The n_{draws} method is simply a mathematical procedure we have developed that allows the broadening of the freezing curves to be predicted by randomly sub-sampling from \bar{g} , which is constrained by experimental data at high particle concentration.

Using the concept of nucleating area introduced in section 3.2, we try to show in section 3.5 how on average, for the modeled illite system, the smaller critical contact angles within the critical contact angle range that contribute to the early freezing onset in the model experience a less significant drop off as the number of draws is reduced vs. the larger contact angles that contribute to the colder portion of the freezing curve. That is because a higher number of draws is required to replicate the behavior of the weaker (larger) contact angles. So all of the references to active sites and variability are meant to be comprehended within the context of the mathematical model. The text referenced by the reviewer has been modified on Page 19/3-15 to reflect this:

“Perhaps the most notable characteristic is how the freezing curves of all three systems analyzed ascend together early as temperature is decreased but then diverge as the temperature decreases further (Figs. 5, 6a, and 7a). The closeness of the data at warmer temperatures (the ascent) is interpreted by the framework as the continued presence of smaller contact angles within the g^* distributions of some of the particles under all the particle concentrations explored in these experiments. Due to the strength of the ice nucleating activity at small contact angles a smaller number of draws is required to capture this region of the contact angle range than the lower activity described by the larger contact angles. This results in a greater diversity in the larger (weaker) contact angles between the particles and is how the model successfully captures the increasing external variability with decreasing surface area. In a later section the claim of more external variability contributing to the

broader curves below the critical area threshold is supported with a closer look at the numerical results from the model.”

Emphasis on the fact that the finding is not physically constrained has been added on Page 28/29 and Page 29/1:

“We stress however that this explanation is not physical and is merely a mathematical interpretation of the experimental trend being observed.”

One could play devil’s advocate and conclude that this paper nicely shows, that the concept of active site number density is not suitable at all to capture immersion freezing in a consistent sense. At a critical surface area (this depends how well known this property is), the active site number density “jumps” and thus has to be corrected by choosing contact angles that fit to the data (i.e. new g^ distribution). Furthermore, this seems different for different compounds. One could argue that this is not very satisfying when describing a physical process.*

The experimental data shown in the paper does show that the concept of active site density may be unable to capture immersion freezing behavior consistently at low surface areas. The framework presented attempts to describe this inconsistency as the diminishing probability that ice nucleating activity between particles of the same surface area can stay the same. Reduction in surface area is leading to a larger spread in the freezing temperature of the droplets, and the framework is constructed to interpret this larger spread as the reduction in probability of particles retaining similar ice nucleating activity.

More specific comments:

p. 3, l. 10: I would re-word this, since “stochastic” does not assume “randomness”: The stochastic framework is based on freezing events that occur randomly across a particle’s surface and can be constrained with a temperature dependent nucleation rate (Pruppacher and Klett, 1997).

We reworded this to say the stochastic framework assumes nucleation can occur with the same probability at any point on the surface. Text has been changed on Page 3/10-12:

“The stochastic framework assumes that freezing occurs with equal probability at any point across a particle’s surface and can be constrained with a temperature dependent ice nucleation rate (Pruppacher and Klett, 1997).”

p. 3, l. 28 – p. 4, l. 7: There are more papers discussing this issue than Ervens and Feingold. It may be fair to include others.

Other references discussing this issue have been added on Page 4/7-8:

“Similar sensitivities of adiabatic parcel models to time dependent freezing were shown in Wright and Petters (2013) and Vali and Snider (2015).”

P. 8, l. 7: Is it justified to smooth the Fornea et al. frozen fraction curve? Looking at their Fig. 6, there are much more bumps in the frozen fraction curve due to the limited number of freezing events. This may affect the fit parameters/interpretation?

For the purposes of what we are trying to show in Section 3.1 we believe that smoothing the Fornea et al. frozen fraction curve is justified. While the data has more bumps than the smooth fit it succeeds in falling within a temperature range predictable by a multi component stochastic model such as the one we present. We recognize that there remained a discrepancy between our model's sensitivity to cooling rate and the sensitivity measured in the experiment and this limited our conclusion that the model parameters have an impact on how the model behaves under different environmental conditions.

p. 9, l. 23-26: In fact, vice versa is also true and maybe even more important: the model parameters are only valid for those specific experimental conditions, since they are derived from a fit.

We have elaborated on the importance of testing model parameters under different environmental conditions to test their validity on Page 9/28-30 and 10/1-3:

“The result emphasizes that how the active sites are modeled has consequences on what physical parameters (e.g. time, temperature, cooling rate) can influence the freezing outcome and observed droplet freezing temperature spectrum (Broadley et al., 2012) and that model parameters need to be tested under different environmental conditions (e.g. different cooling rates) to properly test their validity.”

p. 10, l. 2-5: This sentence is too speculative. One could leave this out without losing anything.

The sentence has been removed as suggested.

p. 11, l. 15-23: How is θ_{c1} derived?

An identical approach to the one described to determine θ_{c2} is used to determine θ_{c1} , by using a least square fit error approach to compare the freezing probabilities computed from Eq. (9) and (10). This detail has been added on Page 11/18-25 and Page 12/1-2:

“The critical contact angles are determined numerically by identifying the range $[\theta_{c1}, \theta_{c2}]$ for which the freezing probability can be approximated using Eq. (10). Figure 3(a) illustrates the process of identifying θ_{c2} . The blue curves represent freezing probabilities computed via integrating Eq. (10) from 0 to a variable θ_{c2} . The red curve is the freezing probability computed from integrating across the full θ range. As θ_{c2} is increased the resultant curve (blue) approaches the curve computed from the full θ range (red). For the example studied in Fig. 3 (same system examined in Section 3.1), a value of $\theta_{c2} = 0.79$ rad results in a least square error below 0.01 for the freezing probability retrieved from Eq. (10) assessed against the freezing probability retrieved from Eq. (9). An identical approach is followed to determine θ_{c1} .”

p. 13, l. 1-6: And this is prone to large uncertainties as discussed above.

We realize that large uncertainties exist in surface area estimates and were ignored in our analysis. We have elaborated on this in our revised manuscript on Page 23/7-30 and Page 24/1-

11:

“One final thing to note is that the mathematical analysis presented here ignores the variability in total particle surface area present between droplets in each experiment. According to the range of droplet diameters mentioned in the Broadley et al. (2012) data of 10-20 μm , surface area variability between the smallest and largest droplets in the experiment can be as high as a factor of 8. This assumes each droplet has the same particle concentration. While for the data presented from the CMU cold plate with droplet diameter varying from 500-700 μm , variability can be as high as a factor of 5. This assumes that the particle concentration is the same in each droplet, as they were produced from well-mixed particle suspensions in water. This surface area variability can be the source of an alternative explanation to the broadness of the freezing curves, whereby an analysis along the lines of what is presented in Alpert and Knopf (2016) can be applied.

The shaded regions of Figs. 5, 6a, and 7a show the predicted temperature range over which freezing of droplets occurs for the surface area variability associated with the diameter range of the considered experiments using \bar{g} (i.e. running Eq. (9) with different values for A). Figs. 5 and 7a show the predicted freezing variability for the highest and lowest mass concentrations while Fig. 6a only shows it for the highest concentration as the range predicted for the lowest concentration almost completely overlaps with the highest concentration. The prediction from surface area variability does contain the temperatures over which droplets freeze for the high concentration freezing curve but falls short of capturing the range for the low concentration-freezing curve. More importantly while the scatter in surface area between droplets can explain some of the broadness in the freezing curves, it is unable to explain why the curves become broader in the temperature range they span with decreasing surface area. Freezing temperature should respond linearly to surface area, if no other factors are changing (Eq. (9)). This observed trend is quite repeatable; according to Broadley et al. (2012) freezing temperatures were reproducible to within 1 K for their illite measurements, while for the CMU experiments for illite, MCC cellulose, and Snomax, the difference in freezing temperature spectra between at least two replicate experiments did not exceed 1 K. Therefore, if surface area scatter alone is proposed to explain the increasing variability of freezing temperatures with decreasing concentration/surface area, a cause for an increase in surface area scatter with decreasing concentration would have to be hypothesized. We recognize that such a surface area variability approach is also a viable one but the framework presented here presents an increase in the variability in ice nucleation activity with decreasing concentration/surface area as the means for describing the observed trends.”

We also show in the Figures below data for low concentration freezing curves of droplets containing cellulose (0.01 wt%) and Snomax (0.08 wt%) retrieved from multiple independent runs:

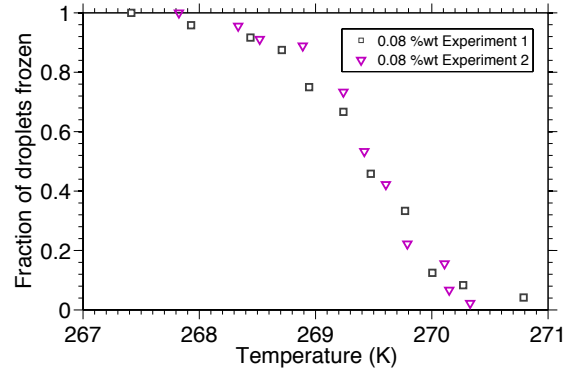


Figure A. Fraction of frozen droplets retrieved from two identical and independent cold plate experiments for droplets containing 0.08 % wt of Snomax.

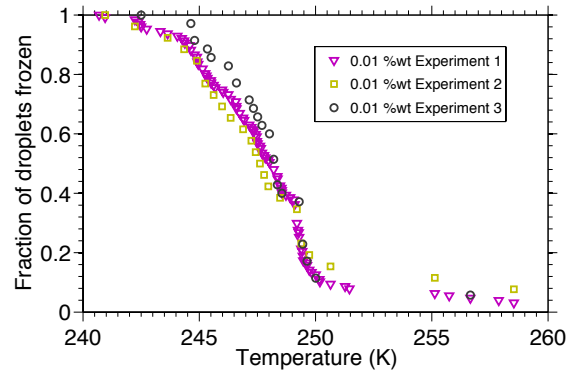


Figure B. Fraction of frozen droplets retrieved from two identical and independent cold plate experiments for droplets containing 0.08 % wt of MCC cellulose.

It can be seen that the values of the fraction of droplets frozen retrieved from multiple independent experiments fall within 1 K of each other.

p. 13, l. 12: You do not know the number of particles in the droplets, but later in the manuscript use these arguments to talk/speculate about internal and external variability. See also p. 14, l. 10-14.

For the purposes of our analysis, the particle population in each droplet is treated as one particle and the total surface area present. Therefore when variability between particles is discussed, the referenced particles are those that have been equated to a population of particles present in each droplet.

This has been clarified on Page 13/10-13:

“For the application of this model to cold plate data where droplets are prepared from a suspension of the species being investigated, the particle population in each droplet is treated as one aggregate surface (and thus one large particle) and a mean surface area value is assumed for the particle material in all the droplets in the array.”

p. 14., l. 26 ...: Having a factor ~2 in droplet diameter variation, results in large uncertainty of surface area excluding variations on the nanoscale. See general comment.

We have addressed the issue of surface area uncertainty and its impact on our analysis. Please see response to two comments above.

p. 14, l. 6: This threshold “concentration” in surface area $7.42 \times 10^{-6} \text{ cm}^2$ is different than the $2 \times 10^{-6} \text{ cm}^2$?

The surface area of $7.42 \times 10^{-6} \text{ cm}^2$ was successfully predicted as being over the critical area while the surface area of $2 \times 10^{-6} \text{ cm}^2$ was better predicted by the random sampling process. Therefore the critical area occurs between these two surface areas. We never meant to imply that the critical area can be a very well defined cut off point, especially given surface area uncertainty. This has been clarified on Page 15/16-20:

“Note that above the threshold concentration A_c , approximated here as occurring between $7.42 \times 10^{-6} \text{ cm}^2$ and $2.02 \times 10^{-6} \text{ cm}^2$, a change in the total available surface area A is all that is required to account for how the change in particle concentration shifts the droplet freezing temperature curve. This is not the case when total area is less than the critical area A_c , as discussed next.”

p. 15, l. 18: Here it is stated 450-550 micrometer in diameter, but figure captions say otherwise. What are the uncertainties in solution concentrations? How much does this result in variation of surface area?

We have fixed typos referring to the range of diameters in our cold plate system to consistently say 500-700 micrometers, as this is the actual range obtained (measured by optical microscopy) in our experiments. We have elaborated on this surface area uncertainty in the experiments analyzed (please see reply to comment above).

p. 15, l. 28: Please add new work on Pseudomonas syringae by Pandey et al. (2016).

A reference to this recent work has been added on Page 16/16-18:

“Its ice nucleation properties are attributed to large protein aggregates, and Snomax is often used as a proxy for atmospheric biological INP (Pandey et al., 2016; Polen et al., 2016; Wex et al., 2015).”

p. 16, l. 7-9: I would expect that with given stochastic and experimental uncertainty, these curves cannot be discriminated. How does this affect your discussion?

The impact that surface area uncertainty has on our discussion is now addressed on Page 23/26-

30 and Page 24/1-11:

“More importantly while the scatter in surface area between droplets can explain some of the broadness in the freezing curves, it is unable to explain why the curves become broader in the temperature range they span with decreasing surface area. Freezing temperature should respond linearly to surface area, if no other factors are changing (Eq. (9)). This observed trend is quite repeatable; according to Broadley et al. (2012) freezing temperatures were reproducible to within 1 K for their illite measurements, while for the CMU experiments for illite, MCC cellulose, and Snomax, the difference in freezing temperature spectra between at least two replicate experiments did not exceed 1 K. Therefore, if surface area scatter alone is proposed to explain the increasing variability of freezing temperatures with decreasing concentration/surface area, a cause for an increase in surface area scatter with decreasing concentration would have to be hypothesized. We recognize that such a surface area variability approach is also a viable one but the framework presented here presents an increase in the variability in ice nucleation activity with decreasing concentration/surface area as the means for describing the observed trends.”

p. 16, l. 21-24: Compared to previous discussion in this manuscript, one would say that the predictions differ from the data, in particular the predictions do not catch the median freezing temperature.

We now mention the discrepancy between the second highest concentration cellulose freezing curve and the \bar{g} model prediction. Text has been modified on Page 17/14-17:

“While the second highest concentration freezing curve’s (0.05 wt%, red) median freezing temperature is not captured by \bar{g} , the broadness of the curve is similar to that predicted by the model and the differences in the median freezing temperatures are within 1 K.”

p. 20, l. 11-14: “Further analysis will show this is not due to an enhancement of ice nucleating activity per surface area but is actually a product of external variability causing a broadening of the ice nucleating spectrum within the droplet ensemble when total surface area is below the critical area threshold.”

See also general comments. This is very speculative and not testable. In fact, following the analysis, it should read: “Further analysis will show this is not due to an enhancement of ice nucleating activity per surface area but is actually a product of changing the distribution to g^ .”*

The statement on Page 20/28-30 and Page 21/1-3 now reads:

“Further analysis will show this is not due to an enhancement of ice nucleating activity per surface area but is actually the random sampling process redistributing smaller and larger contact angles in such a way that some particles now have higher ice nucleating activity per surface area while others have a weaker ice nucleating activity per unit surface area. This is regarded as an

increase in the external variability of the system.”

p. 20, l. 15-23: Here and at other places: Hartmann et al. (2016) also observed this effect of diverging active site number densities. This study deserves to be cited. Also these authors attribute this to erroneous surface areas, similar to the case made by Alpert and Knopf (2016). This also holds for the conclusion section, p. 32, l. 6-8. Hartmann et al. (2016) pointed it already out and gave a convincing argument for it.

We have added text discussing the results of Hartmann et al. (2016) and think they are a powerful tool for going forward in investigating the active site density's potential sensitivity to particle size. This study probes a very different size range than what is probed in our study and looks at a different species. That leaves us curious to see what results would come out if the method of Hartmann et al. (2016) was applied with an extended size range to particle types investigated in our study. Text has been added on Page 27/1-8:

“Hartmann et al. (2016) recently investigated the impact of surface area on active site density of size selected kaolinite particles by probing three different diameters. They concluded that kaolinite ice nucleating activity did not exhibit size dependence, similar to the trends reported here. However a different mineral species was investigated that the illite we focus on here, and they probed a very different size range than in our experiments. We therefore think that our results provide incentive to pursue more of the quite insightful experiments presented by Hartmann et al. (2016) where particle size is varied over a large range.”

p. 22, l. 4-6: This is confusing. At the end it is a surface area effect that governs nucleation. High mass concentration may alter the surface area as stated on lines 18-20.

We have removed our description of the plateauing being a mass concentration effect and not a surface area effect since as the referee pointed out, surface area governs nucleation. The point we are trying to make is that in this high concentration range, there seems to be a physical effect whereby as particles are added coagulation and settling effects are preventing the available surface area from actually increasing. The section now reads on Page 22/19-31 and Page 23/1-6:

“Another important conclusion that can be drawn from this dataset is that high concentration data (0.25 wt%, 0.3 wt%, and 0.5 wt%) exhibited a similar plateauing in freezing temperatures despite additional amounts of illite. This is similar to the concentration range where Broadley et al. (2012) found a saturation effect when further increasing the concentration of illite (over 0.15 wt%). The fact that the concentration where this saturation effect is so similar while the droplet volumes and consequently the amount of illite present between the two systems is quite different points to a physical explanation such as particle settling or coagulation due to the very high occupancy of illite in the water volume. These physical processes could reduce the available particle surface area in the droplet for ice nucleation. Additionally, the high concentration freezing curves show a good degree of broadening in the temperature range over which freezing occurs. These three curves share a similar 50% frozen fraction temperature (with the 0.5 wt% oddly exhibiting a slightly lower 50% frozen fraction temperature than the other two). One explanation that is consistent with the hypothesis of particle settling and coagulation is that it becomes less likely that the droplets contain similar amounts of suspended material when they are generated from such a concentrated suspension (Emersic et al., 2015). This results in larger discrepancies in available surface area between the droplets and therefore a broader temperature range over which the droplets are observed to freeze.”

p. 24, l. 4-6: "...along with finding the critical area, A_c , and n_{draws} ".

The sentence on Page 26/2 now reads:

"...along with finding the critical area, A_c , and n_{draws} ."

p. 24, l. 25 and following: The papers by Knopf and Alpert and Alpert and Knopf could be discussed/mentioned.

The model developed by Alpert and Knopf is now discussed on Page 23/9-17:

"According to the range of droplet diameters mentioned in the Broadley et al. (2012) data of 10-20 μm surface area variability between the smallest and largest droplets in the experiment can be as high as a factor of 8. This assumes each droplet has the same particle concentration. While for the data presented from the CMU cold plate with droplet diameter varying from 500-700 μm , variability can be as high as a factor of 5. This assumes that the particle concentration is the same in each droplet, as they were produced from well-mixed particle suspensions in water. This surface area variability can be the source of an alternative explanation to the broadness of the freezing curves, whereby an analysis along the lines of what is presented in Alpert and Knopf (2016) can be applied."

And on Page 25/19-24:

"Alpert and Knopf (2016) present a single component stochastic framework but successfully describe freezing behavior by considering surface area variability; more specifically they define a distribution of surface areas material in different droplets exhibits. A distribution of particle surface areas can provide a similar basis for variability in freezing temperatures between different particles as a distribution of ice nucleating activity."

p. 24, l. 26-29: These cited CFDC studies likely applied erroneous surface areas that have to be corrected as outlined by Hartmann et al. (2016).

The Hartman et al. (2016) study is now mentioned in this part of this discussion. Please see above comment.

p. 25, l. 23: You mean fig. 9?

Yes, thank you. The typo has been corrected.

p. 26, l. 6: You mean fig. 10?

Yes. Corrected.

p. 25, l. 7: You mean fig. 6?

Yes. Corrected.

p. 25, l. 21-24: For this, the number and size (surface) for particles in each droplet needs to be known which is not the case.

As mentioned in an above comment, the particle population in each droplet is treated as one particle.

p. 28, l. 19: You mean fig. 11?

Yes. Corrected.

p. 28, l. 19: There are no gold and green rectangles.

In text references to the data in the figure are now fixed to match those used in the Figure.

p. 28, l. 28: You mean brown hexagon?

The golden triangles were meant to be referred to here. This is now fixed.

p. 29, l. 4: Alternative explanation given by Alpert and Knopf (2016) could be briefly stated.

These are now included. Please see above comment.

Technical corrections:

p. 13, l. 21: “for an ensemble”

“For an ensemble” has been changed to “for a population”

p. 18, l. 19: “attributed”

p. 42, l. 19: Only circles are from CMU?

p. 43, l. 6: Only circles are from CMU?

p. 45, l. 11: Brown hexagons?

The above corrections have all been made, thank you.

References:

Knopf, D. A. and Alpert, P. A.: A water activity based model of heterogeneous ice nucleation kinetics for freezing of water and aqueous solution droplets, *Farad. Discuss.*, 165, 513–534, doi:10.1039/c3fd00035d, 2013.

Hartmann, S., Wex, H., Clauss, T., Augustin-Bauditz, S., Niedermeier, D., Rösch, M., and Stratmann, F.: Immersion freezing of kaolinite: Scaling with particle surface area, *J. Atmos. Sci.*, 73, 263–278, doi:10.1175/JAS-D-15-0057.1, 2016.

Alpert, P. A. and Knopf, D. A.: Analysis of isothermal and cooling-rate-dependent immersion freezing by a unifying stochastic ice nucleation model, *Atmos. Chem. Phys.*, 16, 2083–2107, 2016, doi:10.5194/acp-16-2083-2016.

Pandey, R., Usui, K., Livingstone, R. A., Fischer, S. A., Pfaendtner, J., Backus, E. H. G., Nagata, Y., Fröhlich-nowoisky, J., Schmüser, L., Mauri, S., Scheel, J. F., Knopf, D. A., Pöschl, U., Bonn, M. and Weidner, T.: Ice-nucleating bacteria control the order and dynamics of interfacial water, *Sci. Adv.*, 2(4), 1–9, doi:10.1126/sciadv.1501630, 2016.

Polen, M., Lawlis, E. and Sullivan, R. C.: The unstable ice nucleation properties of Snomax(R) bacterial particles, *J. Geophys. Res. - Atmos.*, Submitted, 2016.

1 **Effect of particle surface area on ice active site densities retrieved from droplet**
2 **freezing spectra**

3
4 Hassan Beydoun¹, Michael Polen¹, and Ryan C. Sullivan^{1*}

5
6 [1] Center for Atmospheric Particle Studies, Carnegie Mellon University, Pittsburgh PA

7
8 Correspondence to: R. C. Sullivan (rsullivan@cmu.edu)

9
10 *Resubmitted July 12, 2016; Revised September 16, 2016*

Deleted: Revised

11
12
13 **Abstract**

14 Heterogeneous ice nucleation remains one of the outstanding problems in cloud physics
15 and atmospheric science. Experimental challenges in properly simulating particle-
16 induced freezing processes under atmospherically relevant conditions have largely
17 contributed to the absence of a well-established parameterization of immersion freezing
18 properties. Here we formulate an ice active surface site based stochastic model of
19 heterogeneous freezing with the unique feature of invoking a continuum assumption on
20 the ice nucleating activity (contact angle) of an aerosol particle's surface, that requires no
21 assumptions about the size or number of active sites. The result is a particle specific
22 property g that defines a distribution of local ice nucleation rates. Upon integration this
23 yields a full freezing probability function for an ice nucleating particle.

24 Current cold plate droplet freezing measurements provide a valuable and inexpensive
25 resource for studying the freezing properties of many atmospheric aerosol systems. We
26 apply our g framework to explain the observed dependence of the freezing temperature
27 of droplets in a cold plate on the concentration of the particle species investigated.
28 Normalizing to the total particle mass or surface area present to derive the commonly
29 used ice nuclei active surface (INAS) density (n_s) often cannot account for the effects of
30 particle concentration, yet concentration is typically varied to span a wider measureable
31 freezing temperature range. A method based on determining what is denoted an ice
32 nucleating species' specific critical surface area is presented that explains the
33 concentration dependence as a result of increasing the variability in ice nucleating active
34 sites between droplets. By applying this method to experimental droplet freezing data

1 from four different systems we demonstrate its ability to interpret immersion freezing
2 temperature spectra of droplets containing variable particle concentrations.

3 It is shown that general active site density functions such as the popular n_s
4 parameterization cannot be reliably extrapolated below this critical surface area threshold
5 to describe freezing curves for lower particle surface area concentrations. Freezing curves
6 obtained below this threshold translate to higher n_s values, while the n_s values are
7 essentially the same from curves obtained above the critical area threshold; n_s should
8 remain the same for a system as concentration is varied. However, we can successfully
9 predict the lower concentration freezing curves, which are more atmospherically relevant,
10 through a process of random sampling from g distributions obtained from high particle
11 concentration data. Our analysis is applied to cold plate freezing measurements of
12 droplets containing variable concentrations of particles from NX illite minerals, MCC
13 cellulose, and commercial Snomax bacterial particles. Parameterizations that can predict
14 the temporal evolution of the frozen fraction of cloud droplets in larger atmospheric
15 models are also derived from this new framework.

16

17 **1 Introduction**

18 Above water's homogenous freezing temperature near $-38\text{ }^\circ\text{C}$ supercooled cloud
19 droplets can only crystallize on a rare subset of atmospheric aerosol particles termed ice
20 nucleating particles (INP) (Baker and Peter, 2008; Vali et al., 2015). The scarcity of these
21 particles directly affects cloud structure, evolution, and precipitation via inducing the
22 Wegener-Bergeron-Findeisen (WBF) process, where ice crystals rapidly grow at the
23 expense of liquid cloud droplets in mixed-phase clouds. Ice nucleation thus plays a
24 crucial role in determining cloud evolution, lifetime, and properties, creating important
25 feedbacks between aerosols, clouds, precipitation, and climate (Pruppacher & Klett,
26 1997; Rosenfeld et al., 2008). As a result, most precipitation over land is induced by
27 cloud glaciation (Cantrell and Heymsfield, 2005; Mülmenstädt et al., 2015). Accurate
28 representation of cirrus and mixed phase clouds in atmospheric models therefore
29 necessitates properly parameterizing the heterogeneous ice nucleation process (DeMott et
30 al., 2010; Eidhammer et al., 2009; Hoose et al., 2010; Liu and Penner, 2005) for different

1 aerosol source types and compositions that possess a wide range of heterogeneous ice
2 nucleation activities (Phillips et al., 2008, 2012).

3 Great challenges in observing the actual heterogeneous ice nucleation nanoscale
4 process is the main culprit impeding the formulation of a consistent and comprehensive
5 framework that can accurately and efficiently represent heterogeneous ice nucleation in
6 atmospheric models (Cantrell and Heymsfield, 2005); we still do not understand what
7 precisely controls the ice nucleation ability of ice active surface sites that catalyze ice
8 embryo formation. There are currently two competing views on the dominant factors that
9 control the heterogeneous ice nucleation process, the stochastic versus deterministic
10 framework (Niedermeier et al., 2011; Vali, 2014). The stochastic framework assumes that
11 freezing occurs with equal probability at any point across a particle's surface and can be
12 constrained with a temperature dependent ice nucleation rate (Pruppacher and Klett,
13 1997). This effectively yields time dependent freezing and an element of non-
14 repeatability (Vali, 2008). On the other hand in the deterministic framework ice
15 nucleation is dictated by ice active surface sites (Fletcher, 1969; Levine, 1950; Meyers et
16 al., 1992; Sear, 2013). Each active site has a characteristic critical freezing temperature,
17 with the site with the highest critical temperature always initiating crystallization
18 instantly (Vali, 2008). Careful examination of the experimental results published by Vali
19 (2014) indicates that the very nature of the process need not be in contention. These
20 results suggest that there is a strong spatial preference on where nucleation occurs,
21 supporting a model of discrete active sites. However, variability in freezing temperatures
22 still occurs indicating that a stochastic element also exists. Considering several decades
23 of experimental work and theoretical considerations (Ervens and Feingold, 2013; Murray
24 et al., 2012; Vali, 1994, 2014; Vali and Stransbury, 1966; Wright et al., 2013; Wright and
25 Petters, 2013), the role of time has been determined to play a much weaker role than
26 temperature does. It remains to be seen whether the difference is significant enough for
27 time-dependent freezing to be completely omitted in atmospheric models.

28 The debate over how to properly parameterize heterogeneous ice nucleation has
29 important implications on how freezing processes are represented in atmospheric models
30 (Hoose et al., 2010; Hoose and Möhler, 2012; Koop et al., 2000; Phillips et al., 2008,

Deleted: randomly

Deleted: 2008

Deleted: temperature fluctuations

Deleted: occur

Deleted: (Ervens and Feingold, 2013; Murray et al., 2012; Vali and Stransbury, 1966; Vali, 1994, 2014; Wright and Petters, 2013; Wright et al., 2013)

Deleted: (Hoose and Möhler, 2012; Hoose et al., 2010; Koop et al., 2000; Phillips et al., 2008, 2012)

1 [2012](#)), and also reflects our fundamental understanding of this nucleation process. Ervens
2 & Feingold (2012) tested different nucleation schemes in an adiabatic parcel model and
3 found that critical cloud features such as the initiation of the WBF process, liquid water
4 content, and ice water content, all diverged for the different ice nucleation
5 parameterizations. This strongly affected cloud evolution and lifetime. The divergence
6 was even stronger when the aerosol size distribution was switched from monodisperse to
7 polydisperse. [Similar sensitivities of adiabatic parcel models to time dependent freezing](#)
8 [were shown in Wright and Petters \(2013\) and Vali and Snider \(2015\).](#)

9 A new parameterization, [starting from](#) classical nucleation theory, is formulated in this
10 paper. The new framework is stochastic by nature to properly reflect the randomness of
11 ice embryo growth and dissolution, and assumes that an ice nucleating particle can
12 exhibit variability in active sites along its surface, what will be referred to as internal
13 variability, and variability in active sites between other particles of the same species,
14 what will be referred to as external variability. A new method is presented to analyze and
15 interpret experimental data from the ubiquitous droplet freezing cold plate method using
16 this framework, and parameterize these experimental results for use in cloud parcel
17 models. New insights into the proper design of cold plate experiments and the analysis of
18 their immersion freezing datasets to accurately describe the behavior of atmospheric ice
19 nucleating particles are revealed. Based on experimental observations and the new
20 framework we argue that active site schemes that assume uniform active site density such
21 as the popular n_s parameterization – a deterministic framework that assigns an active site
22 density as a function of temperature (Hoose et al., 2008; Vali, 1971) – are unable to
23 consistently describe freezing curves over a wide surface area range. This shortcoming is
24 argued to be one of the causes of the discrepancies in retrieved n_s values of the same ice
25 nucleating species using different measurement methods and particle in droplet
26 concentrations (Emersic et al., 2015; Hiranuma et al., 2015a; Wex et al., 2015).

Deleted: based on

27

28 **2 Classical nucleation theory**

29 Ice nucleation is a fundamentally stochastic process brought about by the random
30 formation, growth, and dissolution of critically sized ice germs that overcome the energy

1 barrier associated with the phase transition (Pruppacher and Klett, 1997; Vali and
2 Stransbury, 1966). A homogenous ice nucleation rate for a given volume of supercooled
3 water can therefore be defined from a Boltzmann type formulation:

$$4 \quad J(T) = C \exp\left(-\frac{\Delta G}{kT}\right) \quad (1)$$

5 where J is the ice nucleation rate and has units of freezing events/(time \times volume). ΔG is
6 the energy barrier to crystallization from liquid water as defined in Pruppacher & Klett
7 (1997) and Zobrist et al. (2007). T is temperature, k the Boltzmann constant, and C is a
8 constant. For typical cloud droplet volumes, a temperature of about -38 °C is typically
9 required for the homogeneous ice nucleation rate to become significantly fast such that
10 freezing occurs within minutes or less. At temperatures between -38 and 0 °C a catalyst is
11 required to initiate freezing of cloud droplets. Certain rare aerosol particles – ice
12 nucleating particles – can act as these catalysts and induce heterogeneous ice nucleation
13 in the atmosphere.

14 In expanding to heterogeneous ice nucleation the simplest approach is to assume that
15 instead of ice germ formation occurring randomly throughout a bulk volume of
16 supercooled water, ice nucleation is initiated on a surface. The surface reduces the
17 nucleation energy barrier ΔG by a factor f , dependent on the contact angle between liquid
18 water and the material. The contact angle θ $[0, \pi]$ is actually a proxy for the water-
19 surface interaction system, with smaller values of θ indicating that the surface is a better
20 nucleant. The surface's measured water contact angle cannot actually be simply used to
21 predict its ice nucleation efficiency. The extreme limit of a contact angle of 0° is
22 therefore a perfect ice nucleant, diminishing the energy barrier fully and immediately
23 inducing freezing at the thermodynamic freezing point of water at 0 °C. The
24 heterogeneous ice nucleation rate for a volume of water containing a total surface area of
25 ice nucleating particles (INP) therefore can be defined as (Pruppacher and Klett, 1997):

$$26 \quad J(T) = C \exp\left(-\frac{f(\theta)\Delta G}{kT}\right) \quad (2)$$

27 where J in this case would be expressed as freezing events/(time \times surface area).

1 The simplest stochastic formulation hypothesizes that the nucleation rate is uniform
2 across the ice nucleating particle's surface, i.e. makes a single contact angle assumption.
3 For a large statistical ensemble of droplet-INP pairings the number of frozen droplets
4 after some time t resembles a first order chemical decay (Pruppacher and Klett, 1997):

$$N_f(T, t) = N(1 - \exp(-J(T)At)) \quad (3)$$

6 where N_f is the fraction of droplets frozen after time t at temperature T , N is the total
7 number of particle-droplet pairings and A is the surface area of each individual ice
8 nucleating particle (assumed to be the same for all particles). Furthermore, a probability
9 of ice nucleation, P_f , at the single droplet-particle level can be defined as:

$$P_f = 1 - \exp(-JAt) \quad (4)$$

11

12 **3 Formulation of g : a continuum approach of active site activity to describe** 13 **heterogeneous ice nucleation**

14 Given the large variability in particle surface composition and structure across any one
15 particle, which in turn determines the activity (or contact angle, θ) of a potential ice
16 nucleating site, a different approach is to assume that the heterogenous nucleation rate
17 will vary along the particle-droplet interface. Since the critical nucleation area ($\sim \text{nm}^2$) is
18 much smaller than the total particle area ($\sim \mu\text{m}^2$), we apply a continuum assumption for
19 the ice active site activity (θ) available across a particle's surface without assumptions
20 about the size or number of active sites per particle surface area. The new resulting
21 probability of freezing is:

$$P_f = 1 - \exp\left(-t \int J dA\right) \quad (5)$$

23 where J is now a freezing rate that is allowed to vary for each specific small segment of
24 the particle's surface area, dA . To define the freezing probability as a function of a
25 contact angle distribution, the surface integral (Eq. 5) is transformed into a line integral
26 via the newly defined g parameter and normalized to the total available surface area:

$$g(\theta) = \frac{1}{A} \frac{dA}{d\theta} \quad (6)$$

27

Field Code Changed

Deleted: ; Vali, 2008

1 and the freezing probability for a droplet-particle pair becomes:

$$2 \quad P_f = 1 - \exp\left(-tA \int_0^\pi J(\theta)g(\theta)d\theta\right) \quad (7)$$

3 g is a probability density function describing the continuous active site density of the
4 ice nucleating particle's surface. This is the first use of a continuum description of ~~ice~~
5 nucleating activity to describe the freezing behavior of an individual particle to our
6 knowledge. Some key unique features of our approach are that the number or size of the
7 individual active sites do not have to be assumed or retrieved in order to predict the
8 freezing probabilities. The causes of these unique features in our framework and the
9 choice of a normal distribution for the contact angle will be explored and justified in a
10 following section.

Deleted: active site density

11 In this work the *internal* variability of an individual ice nucleating particle expresses
12 the heterogeneity of its ice nucleating surface. A wider (larger σ) g distribution describes
13 a greater particle internal variability of ice active surface site properties or contact angles
14 present on that one particle. This is in contrast to the *external* variability of an ice
15 nucleating species or type, which expresses how diverse a population of particles is in
16 their ice nucleation activities. External variability accounts for differences in the g
17 distributions of individual particles between particles of the same type (such as particles
18 composed of the same mineral phases).

19 We hypothesize that experimentally probed systems can be interpreted as exhibiting
20 internal and external variability based on differences in freezing temperatures of different
21 droplets containing the same material, i.e. the freezing temperature spectrum of a droplet
22 array. The model will be shown to provide a conceptual explanation of what this
23 variability, be it internal or external, stems from. We provide this as a potential
24 explanation for discrepancies in the measured values of the popular deterministic scheme
25 n_s (Hoose and Möhler, 2012; Vali, 2014) for different particle concentrations and
26 consequently different measurements methods. In the following sections the model is
27 developed further to shed light on the impact of the g distribution on time dependent
28 freezing, the contrasting internally and externally variable nature of a species' ice
29 nucleating activity, and the dependence of g on particle size.

1

2 3.1 Internal variability and its impact on time dependent freezing

3 To explore the importance of accounting for ice nucleating variability along a single
4 particle's surface (internal variability) we examined the temperature dependent freezing
5 curves of droplets with single large ash particles immersed in them from Fornea et al.
6 (2009). Their experiments were performed with cooling rates of 1 °C/min. Figure 1
7 displays their experimental data (red dots), a single contact angle (θ) fit to their data (red
8 solid line) that assumes no internal variability, and a g distribution fit using multiple θ s
9 (solid blue line) that allows for internal variability. Fornea et al. retrieved their
10 experimental data points by averaging the observed freezing temperature of the same ash
11 particle-droplet pair after multiple freezing cycles. The averaged values are denoted
12 freezing probabilities since they represent the chance of freezing occurring at that
13 temperature. The ash particle diameter was around 300 μm , clearly much larger than
14 atmospheric particle sizes. Five different particle samples of Mount St. Helens Ash were
15 probed in the study; the one that exhibited the broadest range of freezing temperature was
16 chosen for the examination conducted in this section.

17 To fit a g distribution to an empirical freezing curve, a least square error approach is
18 implemented. A matrix of freezing probabilities is generated for all possible g
19 distributions. If the experimental freezing curve has been retrieved from experiments in
20 which the temperature is dictated by a non-constant cooling rate, an expression that
21 satisfies this condition must be used:

$$22 \quad P_f = 1 - \exp\left(-A \int_0^t \int_0^\pi J(T(t), \theta) g(\theta) d\theta dt\right) \quad (8)$$

23 In equation (8) J is a function of time because temperature varies with time. If the cooling
24 rate \dot{T} is constant, a simple change of variable can be applied:

$$25 \quad P_f = 1 - \exp\left(-\frac{A}{\dot{T}} \int_{T_i}^{T_f} \int_0^\pi J(T, \theta) g(\theta) d\theta dT\right) \quad (9)$$

1 Equation (9) is therefore used to fit the constant cooling rate dataset from Fornea et al.
2 (2009) considered here as well as datasets considered later in the paper. $J(T, \theta)$ is
3 evaluated using CNT parameters presented in Zobrist et al. (2007).

4 The g fit performs much better in capturing the behavior of the observed freezing
5 temperature spectrum in Fig. 1, as expected given the greater degrees of freedom allowed
6 for the multiple θ fit. The single θ fit has a steeper dependence on temperature; the
7 double exponential temperature dependence of the freezing probability in Eq. (4) (J is an
8 exponential function of temperature in itself as can be seen in Eq. (2)) results in an
9 approximately temperature step function. The diversity of nucleating ability on the
10 particle surface captured by the g parameter offsets some of the steepness and yields a
11 more gradual freezing curve, more similar to the actual experimental freezing probability
12 curve.

13 Two droplet freezing probability fits (dotted lines) are also plotted in Fig. 1 using the
14 single and multiple θ fits but with a larger cooling rate of 10 K/min. One fit uses the same
15 g distribution used previously, while the additional single θ fit is approximated as a
16 normal distribution with a near zero standard deviation, similar to a Delta Dirac function.
17 The resultant freezing probabilities are then computed and plotted for every T , using Eq.
18 (9). It can be seen that the g fit retains much stronger cooling rate dependence, with the g
19 freezing probability curve shifting about 2 K colder and the single θ curve shifting just
20 0.5 K colder for the faster 10 K/min cooling rate. The 2 K prediction presented here is
21 still smaller than the one retrieved experimentally by Fornea et al. (2009) for varying the
22 cooling rate from 1 K/min to 10 K/min, which was measured to be 3.6 K. However, it is
23 unclear which of the samples presented in their work corresponds to this change in
24 median freezing temperature as it is only mentioned as an average decrease in
25 temperature for all of the different samples tested.

26 This numerical exercise shows that wider g distributions theoretically yield stronger
27 time dependence due to the partial offset of the strong temperature dependence that the
28 nucleation rate in Eq. (2) exhibits. The result emphasizes that how the active sites are
29 modeled has consequences on what physical parameters (e.g. time, temperature, cooling
30 rate) can influence the freezing outcome and predicted droplet freezing temperature

Deleted: 1 under different environmental conditions. Instead of prescribing a cooling rate the freezing probabilities are generated by

Moved down [1]: running Eq. (

Deleted: 7) for the entire temperature range with each fit for $\Delta t = 1$ hour.

Deleted: .

Deleted: time

Deleted: 5

Deleted: warmer

Deleted: 1

Deleted: warmer

Deleted: 1 hour hold time.

Deleted: observed

1 spectrum (Broadley et al., 2012), and that model parameters need to be tested under
2 different environmental conditions (e.g. different cooling rates) to properly test their
3 validity. In Fig. 1 a wider g distribution resulted in a higher sensitivity to cooling rate,
4 which resulted in a shift of the freezing curve to lower temperatures as the system was
5 cooled at a faster rate. This significant change in the freezing probability's sensitivity to
6 temperature is the cause of the more gradual rise in the freezing probability for the
7 system when applying a non-Delta Dirac g distribution. This is effectively enhancing the
8 stochastic element in the particle's ice nucleation properties. The enhancement of the
9 stochastic element brings about a more important role for time as shown in Fig. 1. The
10 finding of this exercise is consistent with previously published work on time dependent
11 freezing such as those reported by Barahona (2012), Wright and Petters (2013), and
12 Herbert et al. (2014) amongst others.

Deleted: . In Fig. 1 a wider g distribution resulted in higher sensitivity to time, which resulted in a shift of the freezing curve to higher temperatures as the system was allowed to temporally evolve at a fixed temperature. This significant change in the freezing probability's sensitivity to temperature is the cause of the more gradual rise in the freezing probability for the system when applying a non-Delta Dirac g distribution. This is effectively enhancing the stochastic element in the particle's ice nucleation properties. The shallower response of freezing probability to decreasing temperature (deterministic freezing) creates a greater opportunity for time-dependent (stochastic freezing) to manifest, as a larger fraction of the droplets spend more time unfrozen. The enhancement of the stochastic element brings about a more important role for time as shown in Fig. 1. The finding of this exercise is consistent with previously published work on time dependent freezing such as those reported by Barahona (2012), Vali and Stransbury (1966), Vali, (1994b), and Wright and Petters (2013), amongst others. -

14 3.2 Defining g as a normal distribution of ice nucleation activity

15 The fit for a particle-freezing curve such as the one considered in the previous section
16 (Fig. 1) does not have a unique solution. There are, mathematically speaking, infinite
17 solutions for the g distributions that produce a representative freezing curve. In any
18 considered distribution an ascending tail with increasing contact angle represents a
19 competition between more active but less frequent surface sites, and less active but more
20 frequent sites. Sites with lower activity and lower frequency have essentially zero chance
21 of contributing to the overall freezing probability, primarily due to the nucleation rate's,
22 J , exponential dependence on the energy barrier to nucleation and the freezing
23 probability's exponential dependence on J as shown in Eqs. (2) and (7). It is therefore
24 sufficient to conceptualize that the particle has a well-defined monotonic spectrum of
25 active sites increasing in frequency while decreasing in strength. The spectrum is
26 modeled as a continuum of ice nucleation activity described by the g distribution, as
27 depicted on the upper right hand corner in Fig. 2. Figure 2 also shows part of the g
28 distribution (the ascending part representing the monotonic spectrum of active sites)
29 retrieved for the case example in section 3.1 (log scale) discretized into numerical bins,
30 where the height of each bin represents the abundance of that θ across the particle's

1 surface. The area in each column thus represents the total surface area with that value of
 2 θ . As in Fig. 2's inset the darker colors are used to emphasize more active ice nucleating
 3 activity at the smaller contact angles.

4 The ascending part of the curve of the normal g distribution covering the smallest
 5 (most active) values of θ in Fig. 2 can therefore capture this active site model. The wider
 6 the defined g distribution (i.e. for a larger standard deviation, σ) the more diverse the
 7 considered system is in its internal variability of ice nucleation activity. Since the
 8 freezing probability is determined solely by a fraction of the ascent of the normal
 9 distribution – as this captures the rare but most active sites that determine the actual
 10 freezing rate J and freezing probability P_f – the following approximation to Eq. (9) can be
 11 made:

$$\begin{aligned}
 12 \quad P_f &= 1 - \exp \left(-\frac{A}{T} \int_{T_i}^{T_f} \int_0^\pi J(T, \theta) g(\theta) d\theta dT \right) \\
 13 \quad &\approx 1 - \exp \left(-\frac{A}{T} \int_{T_i}^{T_f} \int_{\theta_{c_1}}^{\theta_{c_2}} J(T, \theta) g(\theta) d\theta dT \right) \quad (10)
 \end{aligned}$$

14 where θ_{c_1} and θ_{c_2} are the approximate cutoff points in the g distribution that contain the
 15 critical range of the most active contact angles. Outside $[\theta_{c_1}, \theta_{c_2}]$ the less active contact
 16 angles have a negligible contribution to the actual manifested freezing rate and freezing
 17 probability. The critical contact angle range is a strong function of the area of the particle.

18 The critical contact angles are determined numerically by identifying the range
 19 $[\theta_{c_1}, \theta_{c_2}]$ for which the freezing probability can be approximated using Eq. (10). Figure
 20 3(a) illustrates the process of identifying θ_{c_2} . The blue curves represent freezing
 21 probabilities computed via integrating Eq. (10) from 0 to a variable θ_{c_2} . The red curve is
 22 the freezing probability computed from integrating across the full θ range. As θ_{c_2} is
 23 increased the resultant curve (blue) approaches the curve computed from the full θ range
 24 (red). For the example studied in Fig. 3 (same system examined in Section 3.1), a value
 25 of $\theta_{c_2} = 0.79$ rad results in a least square error below 0.01 for the freezing probability

Deleted: captures 99.9% of
Deleted: complete

1 retrieved from Eq. (10) assessed against the freezing probability retrieved from Eq. (9).

2 An identical approach is followed to determine θ_{c1} .

3 Furthermore, the critical contact angle range can be used to estimate a hypothetical
4 nucleating area of the particle – the total active site surface area where nucleation will
5 take place. The nucleation area $A_{nucleation}$ can be estimated as follows:

$$6 \quad A_{nucleation} = A \int_{\theta_{c1}}^{\theta_{c2}} g(\theta) d\theta \quad (11)$$

7 For the large ash particle system analyzed in the previous section (Fig. 1) it is estimated
8 that for its estimated diameter of $300 \mu m$ and a cooling rate of $1 K/min$ $\theta_{c1} \approx 0.4$ rad and
9 $\theta_{c2} \approx 0.79$ rad. Application of Eq. (11) yields a total ice active surface area estimate of
10 27 nm^2 . Classical nucleation theory estimates that the area of a single active site is 6 nm^2
11 (Lüönd et al., 2010; Marcolli et al., 2007). The estimated total area of nucleation is
12 therefore consistent with this value and supports the argument that competition between
13 sites along the critical range of θ is taking place. However, the surface area where ice
14 nucleation is occurring remains a very tiny fraction of the total particle surface. This
15 further justifies the use of a continuum of surface area to define g as $dA/d\theta$ (Eq. 6). The
16 nucleating area is a function of both the g Gaussian distribution of θ , and the total
17 surface area of the considered particle. Figure 3(b) shows the g distribution in log scale
18 and highlights in red the fraction of the distribution covered by the critical contact angle
19 range. It is important to emphasize that the critical contact angles are variable parameters
20 and not a property of the ice nucleating species. Therefore, for the same g distribution the
21 critical contact angles shift in the direction of decreasing activity (larger θ) for smaller
22 surface areas and increasing activity (smaller θ) for larger surface areas.

24 3.3 Using critical area analysis to predict droplet freezing spectra obtained in cold 25 plate experiments

26 Many droplet freezing array experimental methods such as those described in
27 Broadley et al. (2012), Murray et al. (2011), Vali (2014), Wright & Petters (2013), and
28 Hiranuma et al. (2015a) use atmospherically relevant particle sizes (hundreds of

Deleted: found using

Deleted: full range of θ .

Deleted: 10

Deleted: Hiranuma et al. (Hiranuma et al., 2015a) use atmospherically relevant particle sizes (hundreds of nanometers to a few microns in diameter) but create the droplet array from a prepared suspension of the particles of interest in water. The resultant particle concentrations are typically high and the number of particles present in each droplet has to be approximated using statistical methods. When total particle surface area is high enough we hypothesize that it is conceivable that a threshold is reached whereby most of the species' maximum possible external variability is already available within the particle-droplet system. At this point it is approximated that no additional diversity in external variability (ice active site ability or θ) is created by further increasing the total particle surface area in the water volume; the external variability has effectively saturated. For the application of this model to cold plate data where droplets are prepared from a suspension of the species being investigated, the particle population in each droplet is treated as one aggregate surface and a mean surface area value is assumed for particle material in all the droplets in the array. This estimate is retrieved from the weight percentage of the material in the water suspension and our best guess for a reliable surface area density.

1 nanometers to a few microns in diameter) but create the droplet array from a prepared
 2 suspension of the particles of interest in water. The resultant particle concentrations are
 3 typically high and the number of particles present in each droplet has to be approximated
 4 using statistical methods. When total particle surface area is high enough we hypothesize
 5 that it is conceivable that a threshold is reached whereby most of the species' maximum
 6 possible external variability is already available within the particle-droplet system. At this
 7 point it is approximated that no additional diversity in external variability (ice active site
 8 ability or θ) is created by further increasing the total particle surface area in the water
 9 volume; the external variability has effectively saturated. For the application of this
 10 model to cold plate data where droplets are prepared from a suspension of the species
 11 being investigated, the particle population in each droplet is treated as one aggregate
 12 surface (and thus one large particle) and a mean surface area value is assumed for the
 13 particle material in all the droplets in the array. This estimate is retrieved from the weight
 14 percentage of the material in the water suspension and our best guess for a reliable
 15 surface area density which is how much surface area the particle material possesses
 16 relative to its mass (Hiranuma et al., 2015a, 2015b).

17 Past the hypothesized surface area threshold, which will be referred to as the critical
 18 area, each member of the system's population (droplets with particles immersed in them)
 19 become approximately identical in their ice nucleation properties and the theoretical
 20 frozen fraction can be expressed as:

$$F = P_f(\text{one system}) = 1 - \prod_{i=1}^n P_{uf,i} \quad (12)$$

22 where F is the droplet frozen fraction, n is the number of droplets, and $P_{uf,i}$ is the
 23 probability that the droplet i does not freeze. Further expanding the expression yields:

$$F = 1 - \exp \left[-t \left(\sum_{i=1}^n A_i \int_0^{\pi} J(\theta) g_i(\theta) d\theta \right) \right] = 1 - \exp \left[-t \int_0^{\pi} J(\theta) \sum_{i=1}^n (A_i g_i) d\theta \right] \quad (13)$$

25 Next the parameter \bar{g} is defined:

Deleted: particles per droplet

Deleted: particle

1
$$\bar{g} = \frac{\sum_{i=1}^n (A_i g_i)}{A_t} \quad (14)$$

2 where A_i is the sum of all particle surface area available inside a given droplet i , and A_t is
 3 the mean particle surface area per droplet. Equation (13) then becomes:

4
$$\Rightarrow F = 1 - \exp\left(-tA_t \int_0^\pi J(\theta) \bar{g}(\theta) d\theta\right) \quad (15)$$

5 \bar{g} is the arithmetic average of all the g distributions for ensemble of particles in the
 6 droplet (each particle has its own g distribution) with a cumulative area larger than the
 7 critical area of the species they belong to. Alternatively \bar{g} can be thought of as the
 8 probability density function for all possible ice nucleating activity of a given species or
 9 particle type. It is worth mentioning that \bar{g} is a true continuous probability density
 10 function. While the g distribution of an individual particle is an approximate continuous
 11 function – due to the very small size of ice nucleating active sites – \bar{g} contains all
 12 possible values of contact angles that an ice nucleating species can exhibit.

13 Above a certain surface area threshold it is conceptualized that the chance of an ice-
 14 nucleating particle surface not possessing the entire range of ice nucleating activity (θ)
 15 becomes very small. The model therefore assumes that any particle or population of
 16 particles having a total surface area larger than the critical area can be approximated as
 17 having \bar{g} describe the actual g distribution of the individual particles. In other words, for
 18 large particles with more surface area than the critical area threshold, it is assumed that
 19 the external variability between individual particles will be very small such that the
 20 particle population can just be described by one average continuous distribution of the ice
 21 nucleation activity, \bar{g} .

22 To resolve the g distributions of the systems possessing particle surface areas smaller
 23 than the critical area the first step is to approximate the critical area. Experiments must
 24 start at very high particle mass concentrations to ensure the total surface area per droplet
 25 exceeds the critical area. For the illite mineral particle case study considered next, for
 26 example, high particle concentrations were those that resulted in total particle surface
 27 areas greater than about $2 \times 10^{-6} \text{ cm}^2$. The particle number or surface area concentration is

Deleted: A_t
 Deleted: A_i
 Deleted: representing that value of g_i (which is a function of θ).

Deleted: ensemble

Deleted: active site ability

Deleted: active site

Deleted: surface area

Deleted: number of particles and

1 then decreased until the retrieved g distribution (from the measured droplet freezing
2 temperature spectrum for an array of droplets containing particles) can no longer be
3 reasonably predicted by \bar{g} . This point can identify the parameter A_c , the critical area of
4 the species under study. A schematic of the procedure is summarized in Fig. 4.

5 Figure 5 shows experimental freezing curves (open symbols) taken from Broadley et
6 al. (2012), with different particle surface area concentrations. 10-20 μm droplets were
7 used and cooled at a cooling rate of 5 K/min. The curves from the highest particle
8 concentration experiments, $7.42 \times 10^{-6} \text{ cm}^2$ (6b) and $2.02 \times 10^{-6} \text{ cm}^2$ (6a), are used to
9 approximate the critical area of the system by first fitting the 6b curve with a g
10 distribution and then successfully predicting the 6a curve with the same g distribution
11 obtained from 6b and applying a particle surface area correction. The fit to the 6b curve is
12 done using Eq. (9) and follows the same procedure of least square error fitting described
13 in section 3.1. This g distribution is therefore assumed to be the \bar{g} of the considered
14 system with $\mu = 1.72$, and $\sigma = 0.122$. Note that above the threshold concentration A_c ,
15 approximated here as occurring between $7.42 \times 10^{-6} \text{ cm}^2$ and $2.02 \times 10^{-6} \text{ cm}^2$, a change in
16 the total available surface area A is all that is required to account for how the change in
17 particle concentration shifts the droplet freezing temperature curve. This is not the case
18 when total area is less than the critical area A_c , as discussed next.

19 Moving to the lower concentration freezing curves ($1.04 \times 10^{-6} \text{ cm}^2$ – 5a; and 7.11×10^{-7}
20 cm^2 – 4a) the transition to below the critical area begins to be observed. The solid lines
21 attempt to predict the experimental data points using \bar{g} . Predicting experimental data
22 points for the $1.04 \times 10^{-6} \text{ cm}^2$ (5a) system with the same \bar{g} distribution captures the 50%
23 frozen fraction point but fails at accounting for the broadness on the two ends of the
24 temperature spectrum. The prediction from \bar{g} completely deteriorates in quality for the
25 lowest concentration experiments ($7.11 \times 10^{-7} \text{ cm}^2$ – 4a) as it neither captures the
26 temperature range over which freezing is occurring nor the 50% frozen fraction point.

27 We investigated a similar trend when freezing droplets containing commercial
28 Snomax (York International), and MCC cellulose (Sigma-Aldrich) particles immersed in
29 oil in our in-house cold plate system, described by Polen et al. (2016). The relevant

Deleted: around

Formatted: Space After: 0 pt, No widow/orphan control, Don't adjust space between Latin and Asian text, Don't adjust space between Asian text and numbers

1 system details are that particle-containing water droplets of approximately 500-700 μm in
2 diameter are immersed in squalane oil, analogous to the method of Wright et al. (2013),
3 and the droplets' freezing temperature is determined optically during a constant 1 K/min
4 cooling cycle. A new sample solution was prepared of the material being tested before
5 every experiment to avoid potential changes to the ice nucleation ability due to ageing.
6 Ultrapure milli-Q water was used to minimize any background impurities that could
7 provide a source of ice nucleants or solutes that would alter the freezing temperature of
8 the water. Around 50 0.1 μL droplets were then produced with a pipette from this
9 solution. Each freezing experiment was repeated at least twice, with about 50 droplets
10 per run, to confirm that the independently retrieved frozen fractions fall within 1 K of
11 each other for each replicate experiment. Figure 6a shows decreasing concentration
12 freezing curves for droplets containing Snomax particles. Snomax is a freeze-dried
13 powder manufactured from non-viable *Pseudomonas syringae* bacteria and is commonly
14 used to make artificial snow due to its very mild freezing temperature of -3 to -7 $^{\circ}\text{C}$. Its
15 ice nucleation properties are attributed to large protein aggregates, and Snomax is often
16 used as a proxy for atmospheric biological INP (Pandey et al., 2016; Polen et al., 2016;
17 Wex et al., 2015). A similar approach was undertaken in which \bar{g} was retrieved using the
18 highest concentration freezing curve (solid blue line). The surface area density is
19 assumed to be 1 m^2/g though it is recognized that given the protein aggregate based ice
20 nucleating mechanism of Snomax it is difficult to attribute a surface area of nucleation to
21 a mass of Snomax powder. However, a surface area value needs to be assumed to retrieve
22 the ice nucleating properties using the framework presented here for the sake of
23 comparing Snomax to the other systems. For an assumed critical area of $4 \times 10^{-6} \text{ cm}^2$ (the
24 surface area at 0.1 wt%) \bar{g} was found to have $\mu = 0.66$, and $\sigma = 0.055$. Unlike the illite
25 dataset considered first, only 50% of the freezing behavior of the second highest
26 concentration freezing curve is captured by a frozen fraction retrieved from \bar{g} (solid red
27 line). Further lowering the concentration produces a similar trend previously observed for
28 the droplets containing illite, with similar freezing onsets at higher temperatures but
29 significant divergence at lower temperatures (purple and green points). The frozen
30 fractions retrieved from \bar{g} for the 0.08 wt% and 0.07 wt% Snomax droplets (not plotted,
31 as they almost overlap with the solid red line) do not capture any of the freezing behavior

Deleted:

Deleted: 450-550

Deleted: Figure 6

Deleted: (Wex et al., 2015)

1 measured indicating a very sensitive dependence of ice nucleating activity on surface
2 area. A notable difference from the droplets containing illite is that there is significant
3 weakening in ice nucleation ability as the concentration/surface area of Snomax is
4 reduced. This behavior matches what is known regarding the low abundance of the most
5 efficient but fragile Type I ice nucleating proteins that freeze at -3 to -2 °C, versus the
6 more abundant and resilient but less efficient Type III proteins that freeze around -8 to -7
7 °C (Polen et al., 2016; Turner et al., 1990; Yankofsky et al., 1981).

Deleted: active site density

Deleted: A potential explanation for this effect in the context of the framework presented here will be discussed in a following section.

Formatted: Font:Times New Roman, 10 pt

8 The freezing curves from droplets containing MCC cellulose powder (Hiranuma et al.,
9 2015b) are shown in Fig. 7a. For the MCC cellulose freezing curves \bar{g} was found to have
10 $\mu = 1.63$, and $\sigma = 0.12$, from the 0.1 wt% curve. The freezing curve retrieved from
11 droplets containing 0.1 wt% (blue) cellulose was estimated to be the critical area
12 transition value. While the second highest concentration freezing curve's (0.05 wt%, red)
13 median freezing temperature is not captured by \bar{g} , the broadness of the curve is similar to
14 that predicted by the model and the differences in the median freezing temperatures are
15 within 1 K. Assuming a surface area density of 1.44 g/m² (Hiranuma et al., 2015a) the
16 critical area for MCC cellulose is estimated to be around $\sim 9.4 \times 10^{-4}$ cm². MCC cellulose
17 appears to exhibit ice nucleating capabilities reasonably stronger than illite and
18 significantly weaker than Snomax, based on the observed freezing temperature spectra
19 and the \bar{g} values retrieved. \bar{g} for Snomax was 0.66 ± 0.055 , 1.72 ± 0.122 for illite NX, as
20 compared to 1.63 ± 0.12 for MCC cellulose.

Deleted: 7

Deleted: as

Deleted: curve

Deleted: can be

Deleted: directly from \bar{g} .

21 To predict the freezing curves of the droplets with particle surface areas lower than the
22 estimated critical area for the systems considered here, the aggregate surface area of the
23 entire particle population within each droplet is modeled as one large surface. A contact
24 angle θ_r is randomly selected from the full contact angle range $[0, \pi]$, and the value of
25 the active site distribution g^* for the particle i being sampled for at θ_r is assigned the
26 value of $\overline{g(\theta_r)}$:

$$(g_i^*(\theta_{r,ndraw})) = \overline{g(\theta_r)} \quad (16)$$

28 The g^* distributions within this numerical model are given an asterisk to indicate that
29 they are discrete distributions.

1 This process is repeated for a parameter n_{draws} , for each droplet in the array that
 2 produced the freezing curve being modeled. n_{draws} is the only parameter that is optimized
 3 for so the modeled freezing curves can predict the behavior of the experimental freezing
 4 curves. The value of n_{draws} typically ranges from 9 to 65 for the systems analyzed here and
 5 is therefore a relatively soft optimization parameter with small dynamic range. The
 6 sampled g^* distributions are normalized with respect to the estimated total surface area
 7 for the freezing curve being modeled before being used to compute the freezing
 8 probability. The bottom part of Fig. 4 shows a schematic of how g^* is retrieved from \bar{g}
 9 using n_{draws} . With the sampled g^* distributions the freezing probability of each droplet is
 10 calculated using Eq. (9) and the frozen fraction curve is computed from the arithmetic
 11 average of the freezing probabilities:

$$12 \quad F(\text{below critical area}) = \frac{1}{N} \sum_{i=1}^N P_{f_i} \quad (17)$$

13 where N is the number of droplets in the cold plate array.

14 The behavior of the experimental curve is captured using the n_{draws} numerical model in
 15 which random sampling from the ice nucleating spectrum dictated by \bar{g} is carried out to
 16 predict the freezing curve. The dotted lines in Figs. 5, 6a, and 7a are obtained by
 17 sampling from the \bar{g} model to successfully predict the behavior of all the freezing curves.
 18 The early freezing onsets of the lower concentration systems as well as the broadness in
 19 the curves are both captured with the model. After \bar{g} was obtained from the high
 20 concentration data above the critical area threshold, the only parameter that had to be
 21 optimized to produce these accurately predicted freezing curves was n_{draws} . The values of
 22 n_{draws} for the lower concentration freezing curves for each of the systems investigated
 23 here are 21 ($2.02 \times 10^{-6} \text{ cm}^2$), 19 ($1.04 \times 10^{-6} \text{ cm}^2$), and 11 ($7.11 \times 10^{-7} \text{ cm}^2$) for the droplets
 24 containing illite; 65 (0.09 wt%), 48 (0.08 wt%), and 23 (0.07 wt%) for the droplets
 25 containing Snomax; and 21 (0.05 wt%), 11 (0.01 wt%), and 9 (0.001 wt%) for the
 26 droplets containing cellulose. It should also be noted that there is an n_{draws} value for each
 27 system above for which the sampled distribution mimics \bar{g} . For example, when n_{draws} is
 28 25 for the illite system the retrieved distribution will produce a freezing curve equivalent
 29 to using \bar{g} .

Deleted: 6

Deleted: 7

1 Perhaps the most notable characteristic is how the freezing curves of all three systems
 2 analyzed ascend together early as temperature is decreased but then diverge as the
 3 temperature decreases further (Figs. 5, 6a, and 7a). The closeness of the data at warmer
 4 temperatures (the ascent) is interpreted by the framework as the **continued** presence of
 5 **smaller contact angles (stronger active sites) within the g^* distributions of some of the**
 6 **particles** under all the particle concentrations explored in these experiments. **Due to the**
 7 **strength of the ice nucleating activity at small contact angles a smaller number of draws**
 8 **is required to capture this region of the contact angle range than the lower activity**
 9 **described by the larger contact angles.** This **results in a greater diversity in the larger**
 10 **(weaker) contact angles between the particles and is how the model successfully captures**
 11 **the increasing external variability with decreasing surface area.** In a later section the
 12 claim of more external variability contributing to the broader curves below the critical
 13 area threshold is supported with a closer look at the numerical results from the model.

14 The droplets containing Snomax displayed an immediate shift in freezing behavior for
 15 small changes in concentration (from 0.1 wt% to 0.09 wt%) whereby a small drop in
 16 concentration and thus surface area resulted in a broader temperature range over which
 17 freezing of the droplets occurred (Fig. 6a). In the context of the model presented here this
 18 is due to the mode of the \bar{g} distribution occurring at a very small (and thus very active)
 19 contact angle of 0.66. In this contact angle range the barrier to nucleation is greatly
 20 reduced causing freezing to be even more sensitive to the strongest active sites, and less
 21 sensitive to the competing active sites that are weaker but more abundant (depicted in
 22 Fig. 2), and therefore causing freezing curves to be quite steep versus T . A small change
 23 in the surface area of this material may have produced a significant reduction in the
 24 probability of droplets possessing **this very strong range of ice nucleating activity,**
 25 resulting in the observed broadening of the freezing curves. This trend in Snomax is
 26 further investigated **numerically** in a following section.

27 Figure 4 also plots the popular exclusively deterministic scheme's ice active site
 28 density parameter n_s (Hiranuma et al., 2015a; Murray et al., 2012; Vali, 1971, 2008; Wex
 29 et al., 2015). n_s is an active site density function defined in the following equation:

30
$$F = 1 - \exp(-n_s(T)A) \quad (18)$$

- Deleted:** some rare high activity
- Deleted:** particle population
- Deleted:** At lower temperatures it appears that there is a wider diversity in the activity of droplets that did not contain these rare efficient active sites, and thus there is significant spread in
- Deleted:** freezing curve for $T < 242$ K. In the context of the framework presented here this can be attributable to strong external variability
- Deleted:** population, with very strong/active nucleators causing similar freezing onsets for different particle concentrations
- Deleted:** the warmer temperatures, and a lack
- Deleted:** strong nucleators explaining the less consistent freezing of the unfrozen droplets at lower temperature. Thus it follows that there is a wider spread in the freezing curves for these droplets, as their freezing temperature is highly sensitive
- Deleted:** the presence of moderately strong active sites.
- Deleted:** expresses
- Deleted:** external variability – the active site density possessed by individual particles from the same particle source

- Deleted:** these
- Deleted:** nucleators

1 Equation (18) is similar in mathematical form to Eq. (15) and inherently assumes that
2 active site density can be defined as uniform over a particle's surface and is therefore
3 independent of the total surface area (it is multiplied by total surface area to estimate total
4 heterogeneous ice nucleation activity). From this point onwards n_s is regarded as the
5 deterministic analog of \bar{g} , where any time-dependent (stochastic) freezing is omitted. The
6 justification presented for the definition and use of the critical area quantity also applies
7 to the n_s framework, where it is argued that n_s ceases to become a proper representation of
8 the ice nucleation activity below the critical area threshold.

9 The values of n_s were retrieved directly from freezing curves of droplets with illite
10 particles immersed in them measured in a cold plate system by Broadley et al. (2012) and
11 used to produce the right panel in Fig. 4. As the total particle surface area of the system
12 under study is reduced from the blue to the red curve, the retrieved n_s values are similar
13 indicating that variability of active sites remains constrained within droplets. Note that
14 both the red and blue curves were obtained from systems we have determined were above
15 the critical area threshold (Fig. 4). Further reduction of total surface area to below the
16 critical area threshold shifts the n_s values noticeably, as seen by the significant increase in
17 $n_s(T)$ for the green curve. As all three curves were obtained by just varying the particle
18 concentration of the same species the same n_s values should be retrieved for all three
19 curves at each temperature; the n_s scheme is designed to normalize for the total surface
20 area or particle mass present. This is successful for the higher particle surface area
21 systems (red and blue curves are similar) but not at lower particle area (green curve
22 diverges). The large increase in n_s observed when total surface area is below the critical
23 area threshold indicates that the observed droplet freezing temperature spectra do not just
24 linearly scale with particle concentration or surface area. Further analysis will show this
25 is not due to an enhancement of ice nucleating activity per surface area but is actually the
26 random sampling process redistributing smaller and larger contact angles in such a way
27 that some particles now have higher ice nucleating activity per surface area while others
28 have a weaker ice nucleating activity per unit surface area. This is regarded as an increase
29 in the external variability of the system.

Deleted: a product of external variability causing a broadening of the ice nucleating spectrum within the droplet ensemble when total surface area is below the critical area threshold.

1 We have observed other similarly large effects of particle concentration on the
2 measured droplet freezing temperature spectrum and the retrieved n_s curves from our own
3 cold plate measurements. Figures 6b and 7b display n_m (active site density per unit mass
4 (Wex et al., 2015)) and n_s curves versus temperature for freezing droplets containing
5 Snomax and MCC cellulose, respectively. Similar to the data in Fig. 4b, these two
6 systems also exhibit a divergence in n_s (or n_m) as concentration (or surface area) is
7 decreased. Droplets containing MCC cellulose exhibited a much stronger sensitivity to
8 decreasing surface area than the droplets containing illite did, with changes in the values
9 of n_s of up to four orders of magnitude. The droplets containing Snomax on the other
10 hand were less sensitive to changes in surface area and exhibited an opposite trend in n_m ,
11 with the values of n_m decreasing with decreasing concentration. This is consistent with
12 the analysis of the Snomax freezing curves, where the ice nucleating activity experienced
13 a substantial drop with decreasing surface area. It is further argued in a later section that
14 this is due to the very sharp active site density function g that Snomax particles appear
15 to possess, resulting in steep droplet freezing temperature curves.

16 In assessing the three systems investigated here, it appears that the critical area
17 threshold depends a lot on the strength ($\overline{g(\theta)}$) of the ice nucleating activity for that
18 system. Capturing the critical area transition for illite required probing droplets that were
19 an order of magnitude smaller than the droplets containing Snomax and cellulose,
20 indicating a very large difference in the scale of the critical area. One explanation for this
21 behavior is that when ice nucleating activity is weak, nucleation can occur over a larger
22 total nucleating surface area. This means there is a smaller chance of losing critical active
23 sites in a droplet as the amount of material is reduced with decreasing particle
24 concentration. This argument is supported by these three data sets that span almost the
25 entire heterogeneous ice nucleation temperature range.

26 For the illite mineral suspensions Broadley et al. (2012) identified two total surface
27 area regimes by analyzing their droplet freezing curves. In the lower surface area regime
28 they observed a different freezing dependence on particle surface area than at higher
29 surface areas. At higher surface areas they saw no dependence of the freezing curves on
30 total particle surface area, which is inconsistent with both the stochastic and deterministic

1 frameworks. For larger droplets the transition seemed to occur at higher total particle
2 surface area indicating that there might be a particle concentration effect impacting the
3 total particle surface area per droplet. We have conducted our own illite measurements on
4 the same mineral sample used by Hiranuma et al. (2015) (Arginotec, NX nanopowder) to
5 investigate this high concentration regime and further probe the applicability of \bar{g} to
6 freezing curves above the identified critical area threshold. Figure 8 shows the frozen
7 fractions versus temperature for an ensemble of droplets containing illite NX on our cold
8 plate system. The concentrations used were 0.5 wt%, 0.3 wt, 0.25 wt%, 0.2 wt%, 0.1
9 wt%, 0.05 wt%, 0.03 wt%, 0.01 wt%, and 0.001 wt% and the droplets were cooled at a
10 rate of 1 K/min. Average surface area estimates are made by assuming 600 μm diameter
11 droplets and a surface area density of 104 m²/g (Broadley et al., 2012). The solid lines are
12 applications of Eq. (15) with the same \bar{g} as the one found for the illite data set considered
13 above. It can be seen that this \bar{g} retrieved from cold plate experiments where droplets are
14 on the order of 10-20 μm produces reasonable predictions of the freezing curves where
15 droplets are on the order of 600 μm and thus contain particle surface areas up to five
16 orders of magnitudes larger. Another important conclusion that can be drawn from this
17 dataset is that high concentration data (0.25 wt%, 0.3 wt%, and 0.5 wt%) exhibited a
18 similar plateauing in freezing temperatures despite additional amounts of illite. This is
19 similar to the concentration range where Broadley et al. (2012) found a saturation effect
20 when further increasing the concentration of illite (over 0.15 wt%). The fact that the
21 concentration where this saturation effect is so similar while the droplet volumes and
22 consequently the amount of illite present between the two systems is quite different
23 points to a physical explanation such as particle settling or coagulation due to the very
24 high occupancy of illite in the water volume. These physical processes could reduce the
25 available particle surface area in the droplet for ice nucleation. Additionally, the high
26 concentration freezing curves show a good degree of broadening in the temperature range
27 over which freezing occurs. These three curves share a close 50% frozen fraction
28 temperature (with the 0.5 wt% oddly exhibiting a slightly lower 50% frozen fraction
29 temperature than the other two). One explanation that is consistent with the hypothesis of
30 particle settling and coagulation is that it becomes less likely that the droplets contain
31 similar amounts of suspended material when they are generated from such a concentrated

Deleted: 500

Deleted: 500

Deleted:

Deleted: This supports the hypothesis that the high surface area regime for illite experiments is actually experiencing a particle mass concentration effect and not a total surface area effect.

1 suspension (Emersic et al., 2015). This results in larger discrepancies in available surface
2 area between the droplets and therefore a broader temperature range over which the
3 droplets are observed to freeze.

4 One final thing to note is that the mathematical analysis presented here ignores the
5 variability in total particle surface area present between droplets in each experiment.
6 According to the range of droplet diameters mentioned in the Broadley et al. (2012) data
7 of 10-20 μm surface area variability between the smallest and largest droplets in the
8 experiment can be as high as a factor of 8. This assumes each droplet has the same
9 particle concentration. While for the data presented from the CMU cold plate with droplet
10 diameter varying from 500-700 μm , variability can be as high as a factor of 5. This
11 assumes that the particle concentration is the same in each droplet, as they were produced
12 from well-mixed particle suspensions in water. This surface area variability can be the
13 source of an alternative explanation to the broadness of the freezing curves, whereby an
14 analysis along the lines of what is presented in Alpert and Knopf (2016) can be applied.

15 The shaded regions of Figs. 5, 6a, and 7a show the predicted temperature range over
16 which freezing of droplets occurs for the surface area variability associated with the
17 diameter range of the considered experiments using \bar{g} (i.e., running Eq. (9) with different
18 values for A). Figs. 5 and 7a show the predicted freezing variability for the highest and
19 lowest mass concentrations while Fig. 6a only shows it for the highest concentration as
20 the range predicted for the lowest concentration almost completely overlaps with the
21 highest concentration. The prediction from surface area variability does contain the
22 temperatures over which droplets freeze for the high concentration freezing curve but
23 falls short of capturing the range for the low concentration-freezing curve. More
24 importantly while the scatter in surface area between droplets can explain some of the
25 broadness in the freezing curves, it is unable to explain why the curves become broader in
26 the temperature range they span with decreasing surface area. Freezing temperature
27 should respond linearly to surface area, if no other factors are changing (Eq. (9)). This
28 observed trend is quite repeatable; according to Broadley et al. (2012) freezing
29 temperatures were reproducible to within 1 K for their illite measurements, while for the
30 CMU experiments for illite, MCC cellulose, and Snomax, the difference in freezing

Moved (insertion) [1]

1 temperature spectra between at least two replicate experiments did not exceed 1 K.
2 Therefore, if surface area scatter alone is proposed to explain the increasing variability of
3 freezing temperatures with decreasing concentration/surface area, a cause for an increase
4 in surface area scatter with decreasing concentration would have to be hypothesized. We
5 recognize that such a surface area variability approach is also a viable one but the
6 framework presented here presents an increase in the variability in ice nucleation activity
7 with decreasing concentration/surface area as the means for describing the observed
8 trends.

9 10 **3.4 Comparison between \bar{g} , n_s , and other existing parameterizations of** 11 **heterogeneous ice nucleation**

12 To our knowledge, this is the first heterogeneous ice nucleation parameterization that
13 aims to attribute a surface area dependence to active site distributions of ice nucleating
14 particles. The popular exclusively deterministic scheme (Broadley et al., 2012; Murray et
15 al., 2012; Vali, 1994, 2008; amongst others) prescribes an ice active site density function
16 n_s that is an intensive property of the species under study. Equation (15), derived from
17 classical nucleation theory and used in the \bar{g} model, and the deterministic-based Eq. (18)
18 used in the n_s model, have a very close mathematical form. Both carry a negative
19 exponential dependence on surface area, and the temperature dependence in the rest of
20 the variables is inside the exponential.

21 Fitting freezing curves with droplets below the critical area threshold with n_s yields
22 errors similar to fitting the curves with \bar{g} . Doing so has an inherent assumption of the ice
23 nucleation activity being totally internally variable. This is clear in comparing Eqs. (15)
24 and (18). That is \bar{g} and n_s both offer incomplete information about the distribution of ice
25 nucleation activity for a species. A similar conclusion along these lines was reached by
26 Broadley et al. (2012) when the authors noted that the best fits to their freezing curves at
27 low concentrations were achieved when the system was assumed to be totally externally
28 variable. That is when each particle was assumed to have a single contact angle but a
29 distribution assigned a spectrum of contact angles for each particle in the population.

1 There are other formulations that hypothesize an active site based or multi-component
2 stochastic model such as the ones described in Vali & Stransbury (1966), Niedermeier et
3 al. (2011), Wheeler and Bertram (2012), and Wright and Petters (2013). Vali and
4 Stransbury (1966) were the first to recognize that ice nucleating surfaces are diverse and
5 stochastic and thus active sites need to be assigned both a characteristic freezing
6 temperature as well as a variability parameter around that temperature. Niedermerier et
7 al. (2011) proposed the soccer ball model, in which a surface is partitioned into discrete
8 active sites with each site conforming to classical nucleating theory. Marcolli et al.
9 (2007) found a Gaussian distribution of contact angles could best describe their
10 heterogeneous ice nucleation data in a completely deterministic framework. Welti et al.
11 (2012) introduced the alpha-PDF model where a probability density function prescribes
12 the distribution of contact angles that a particle population possesses, such that each
13 particle is characterized by a single contact angle. Wright and Petters (2013)
14 hypothesized the existence of a Gaussian probability density function for a specific
15 species, which in essence is similar to the \bar{g} framework described here. The notable
16 difference is that their probability density function was retrieved via optimizing for all
17 freezing curves, and not from independently fitting high concentration freezing curves as
18 we have done here. Alpert and Knopf (2016) present a single component stochastic
19 framework but successfully describe freezing behavior by considering surface area
20 variability; more specifically defining a distribution of surface areas material in different
21 droplets exhibits. A distribution of particle surface areas can provide a similar basis for
22 variability in freezing temperatures between different particle containing droplets as a
23 distribution of ice nucleating activity.

Deleted: fluctuations

24 The n_s scheme is now more commonly used to describe and compare cold plate and
25 other experimental ice nucleation data instead of the multi-component stochastic schemes
26 (Hiranuma et al., 2015a; Hoose and Möhler, 2012; Murray et al., 2012; Wex et al., 2015).
27 This is in part due to the necessary inclusion of more variables required by other
28 frameworks (such as prescribing a discrete number of active sites in the soccer ball model
29 by Niedermeier et al. (2011)) than the simpler purely deterministic scheme of n_s . The new
30 formulation described here requires only prescribing a species' heterogeneous ice
31 nucleation ability as a function \bar{g} along with finding the critical area, A_{c^*} and n_{draws} . The

Deleted: .

1 critical area is determined by repeatedly measuring freezing curves for the same system
2 or sample using different particle concentrations. Varying particle concentration is
3 already routinely used in cold plate experiments to widen the droplet freezing
4 temperature range that can be measured. An estimate of the total surface area of the
5 particles under study must be made and associated with the retrieved freezing curves.
6 While a process of random sampling using n_{draws} is initially necessary to predict the
7 freezing curves at more atmospherically realistic concentrations below the critical area, in
8 a following section we will introduce easy to apply parameterizations that derive from
9 this sub-sampling of droplet freezing temperature spectra obtained above the critical area
10 threshold.

Deleted: obtain

11

12 **3.5 Dependence of g on ice nucleating particle size**

13 The particle size dependence of the freezing probability comes from the exponential
14 dependence of the freezing probability on the surface area A as shown in Eq. (7). The
15 freezing probability's sensitivity to surface area is the same as its sensitivity to time
16 however the quadratic dependence of area on radius makes size a more sensitive
17 parameter than time. Furthermore, there might be more subtle size dependencies in the g
18 function itself. For a given particle type, whether size affects the diversity (internal
19 variability) of nucleating sites is not something that can be trivially probed
20 experimentally. To accurately test any potential size dependence, particles of varying
21 sizes need to be probed individually and compared. Measurements in which particles
22 were size selected before assessing their ice nucleation ability have been performed, such
23 as those using continuous flow diffusion chambers as described in Koehler et al. (2010),
24 Lüönd et al. (2010), Sullivan et al. (2010a), Welti et al. (2009), among others. However, a
25 similar limitation to the cold plate experiments presents itself in which the freezing onsets
26 of many droplets containing a range of particle sizes are averaged to find a frozen
27 fraction curve. The resultant curves have potential internal and external variability
28 embedded, with not enough information to disentangle them. Hartmann et al. (2016)
29 recently investigated the impact of surface area on active site density of size selected
30 kaolinite particles by probing three different particle diameters. They concluded that

1 kaolinite ice nucleating activity did not exhibit size dependence, similar to the trends
2 reported here. However, a different mineral species was investigated than the illite we
3 focus on here, and they probed a very different size range than in our experiments. We
4 therefore think that our results provide incentive to pursue more of the quite insightful
5 experiments presented by Hartmann et al. (2016) where particle size is varied over a large
6 range.

7 The argument for the existence of a species' specific critical area can be made for
8 either a total number of particles in a specific size range or a total particle surface area.
9 Assuming that a single species' surface area does not undergo intensive changes in its ice
10 nucleation properties (such as chemical processing as discussed in Sullivan et al. (2010a,
11 2010b)) a cut-off critical size can be defined. Above this critical size the active site
12 distribution is \bar{g} while below it is some distribution of g 's that can be sampled from \bar{g} . In
13 one of the cases studied here in Fig. 5 for illite mineral particles the critical surface area
14 was around 10^{-6} cm². This corresponds to a single spherical particle with an equivalent
15 diameter of around 10 μ m, a size cutoff that is quite atmospherically relevant (DeMott et
16 al., 2010). The vast majority of the atmospheric particle number and surface area
17 distributions are found at sizes smaller than 10 μ m. Thus we conclude that for illite
18 mineral particles, individual atmospheric particles will not contain the entire range of ice
19 active site activity (\bar{g}) within that one particle, and each particle's ice nucleation ability is
20 best described by an individual g distribution (that is a sub-sample of \bar{g}).

21 Application of Eq. (11) to find $A_{nucleation}$ for illite systems 6a (2.02×10^{-6} cm²) and 5a
22 (1.04×10^{-6} cm²) from Broadley et al. (2012) gives insight into how the nucleating area is
23 influencing the shape of the freezing curves. System 6a is where the critical area cutoff
24 was found to occur while 5a started to exhibit the behavior of a broader freezing curve
25 with a similar onset of freezing, indicating it is below the critical surface area. In Fig. 9
26 the average cumulative ice nucleating area computed from Eq. (11) is plotted against the
27 critical contact angle range for the two systems. In examining the cumulative nucleating
28 areas two regions can be identified. The first region (0.95 rad to 1.15 rad) includes the
29 stronger active sites that contribute to the earlier warmer regions of the freezing curves,
30 while the second region (1.15 to 1.2) contributes to the tail and colder end of the freezing

Deleted: but with a diverging tail

Deleted: 6

Deleted: The

1 curves. The first region is broader in contact angle range but smaller in total nucleating
2 area. Therefore, statistically there is a higher chance of particles of smaller area to draw
3 these contact angles in the random sampling process. The second region is narrower in
4 the critical contact angle range but occupies a larger fraction of the total nucleating area.
5 Therefore, more draws are necessary to replicate the nucleating behavior of this region
6 and thus there is a stronger drop off in the nucleating area represented by these less active
7 contact angles as the surface of the particles is reduced.

8 This helps to explain why the onset of freezing for the two curves is so similar. The
9 diverging tail can be attributed to the divergence of the nucleating areas at higher contact
10 angles in the critical contact angle range. The steeper rise of the average nucleating area
11 of system 6a is due to its greater chance of possessing active sites characterized by the
12 second region of the critical contact angle range compared to system 5a due to the larger
13 surface area present in 6a. This creates a larger spread in the freezing onset of droplets in
14 system 5a after a few droplets initiated freezing in a similar manner to system 6a.

15 A similar nucleating area analysis was performed on the droplets containing Snomax
16 and is shown in Fig. 10. The cumulative nucleating areas for the droplets with Snomax
17 concentrations of 0.09 wt% and 0.08 wt% (red and green data in Fig. 6, respectively) are
18 calculated and shown over the critical contact angle range with the same color scheme.
19 Unlike the illite system, droplets containing Snomax exhibit a more straightforward trend
20 in cumulative nucleating area vs. critical contact angle. The cumulative nucleating area is
21 consistently smaller in the 0.08 wt% system compared to the 0.09 wt% experiment,
22 indicating that as the particle surface area is reduced the strong nucleators are reduced
23 uniformly over the critical contact angle range. This supports the idea that the range of
24 ice nucleating activity is much smaller for this very ice active system. The consistent
25 decline in nucleating area is attributable to the very narrow critical contact angle range
26 the nucleating area covers (only 0.05 rad). We propose that this is what explains the
27 decrease in n_m with decreasing concentration observed in Fig. 5. We stress however that
28 this explanation is not physical and is merely a mathematical interpretation of the
29 experimental trend being observed.

- Deleted: at low contact angles is strikingly close between the two systems. This is because
- Deleted: the
- Deleted: possessing rare and highly active sites in an ensemble as large as system 5a is high as
- Deleted: occupy a small portion of the total particle area but have a substantial impact on the freezing behavior. This explains why the onset of freezing for the two curves is so similar. The diverging tail can be attributed to the divergence of the nucleating areas at higher
- Deleted: . The steeper rise
- Deleted: average
- Deleted: system 6a is due to its greater chance of possessing moderately strong
- Deleted: sites compared to system 5a due to the larger
- Deleted: area present in 6a.
- Moved down [2]: This creates a larger spread in the freezing onset of droplets in system 5a after a few droplets initiated freezing in a similar manner to system 6a.
- Moved (insertion) [2]

- Deleted: 12
- Deleted: 8

- Deleted: active site

1 The implications of this analysis on the size dependence of g is that below the critical
2 surface area particles may or may not possess freezing behavior similar to the particles
3 above the critical area threshold. The broadening of the freezing curves in the systems
4 analyzed here as the surface area is reduced is interpreted as heterogeneity in ice
5 nucleating ability between the different particles (external variability) and not due to the
6 internal variability within the individual particles themselves. While the broadness of the
7 curves above the critical surface area can be attributed to internal variability, the
8 additional broadness in curves below the critical area cutoff are a result of external
9 variability.

10 More detailed analysis studying various atmospherically relevant ice nucleating
11 particles needs to be done to shed light on whether a particle size cutoff corresponding to
12 a critical area threshold can be used to describe the behavior of different species. This has
13 important implications on whether one active site density function (i.e. \bar{g} or n_s) is
14 sufficient to accurately represent the species' ice nucleating properties in cloud or
15 atmospheric models. If not, a more detailed parameterization resolving the multi-
16 dimensional variability may be necessary, such as a series of g distributions. For illite it
17 seems that external variability is dominant and thus one active site distribution or n_s
18 parameterization does not properly represent the species' ice nucleation behavior. The
19 critical area effect is even more substantial for cellulose and Snomax as their ice
20 nucleating activity is much stronger than illite. However, if a system's global
21 \bar{g} distribution is obtained then its full ice nucleation behavior is contained within and can
22 be successfully subsampled from \bar{g} .

23 Cold plate experimental data potentially provides sufficient information to describe
24 heterogeneous ice nucleation properties in cloud parcel and atmospheric models, however
25 the analysis undertaken here suggests that retrieving one active site density
26 parameterization (e.g. n_s) and applying it to all surface areas can result in misrepresenting
27 the freezing behavior. When samples are investigated, probing a wide concentration
28 range enables the determination of both general active site density functions (e.g. \bar{g}) as
29 well as the behavior of the species' under study at more atmospherically relevant
30 concentrations below the critical area threshold. Once this analysis is undertaken more

Deleted: or \bar{g}

Deleted: Cold plate droplet freezing measurements thus remain a crucial tool for unraveling the complex behavior of ice nucleating particles, particularly when a large particle concentration range is probed.

Formatted: Highlight

Deleted:

1 comprehensive parameterizations can be retrieved as will be developed in the next
2 section.

3 The critical area analysis ~~therefore~~ emphasizes the dangers in extrapolating the
4 freezing behavior of droplets containing a large concentration of ~~particles~~ to droplets
5 containing smaller concentrations or just individual particles. Applying a
6 parameterization such as n_s directly to systems below the critical area threshold in a cloud
7 parcel model for example yields large differences in the predictions of the freezing
8 outcome of the droplet population. As the concentration of the species within the droplets
9 was decreased in the cold plate freezing spectra considered here the actual freezing
10 temperature curves diverged more and more from those predicted when the systems were
11 assumed to be above the critical area. This led to significant changes in the retrieved n_s
12 values, as shown in Figs. 4, 6b, and 7b. The large effects of concentration on the droplet
13 freezing temperature can be directly observed in the frozen fraction curves plotted in
14 Figs. 5, 6a, and 7a. Differences between observed frozen fraction curves and ones that
15 assumed uniform active site density yielded errors in the temperature range the droplets
16 froze over as well as the median droplet freezing temperature. Therefore, a cloud parcel
17 model would be unable to accurately predict the freezing onset or the temperature range
18 over which freezing occurs using a single n_s curve obtained from high concentration data.
19 This has important consequences for the accurate simulation of the microphysical
20 evolution of the cloud system under study such as the initiation of the Wegener–
21 Bergeron–Findeisen and the consequent glaciation and precipitation rates (Ervens *et al.*,
22 [2011](#); Ervens and Feingold, 2012).

23 Figure [11](#) shows the range of n_s values for illite NX mineral compiled from seventeen
24 measurements methods used by different research groups, the details of which are
25 described by Hiranuma *et al.* (2014). The range of data is summarized into shaded
26 sections to separate suspended droplet freezing techniques (such as a cold plate) from
27 techniques where the material under investigation is aerosolized before its immersion
28 freezing properties are assessed (such as the CFDC or AIDA cloud expansion chamber).
29 The aerosol techniques tend to produce higher retrieved n_s values than those obtained by
30 the wet suspension methods. n_s data spanning a surface area range of about five orders of

Deleted: carried out in this paper

Deleted: particle

Field Code Changed

Deleted: ; Ervens *et al.*, 2011

Deleted: 13

1 magnitude retrieved exclusively from both our cold plate measurements and Broadley et
2 al. (2012) measurements are also plotted. Data presented in Fig. 8 that was consistent
3 with a \bar{g} treatment is plotted as n_s (described in the CMU column in Fig. 11). These two
4 datasets along with what was identified as the critical area dataset from the Broadley et
5 al. experiments follow a consistent n_s line that lies within the range of the suspended
6 droplet techniques. The blue triangles are low surface area data points retrieved from
7 dataset 4a from the Broadley et al. measurements. As was argued earlier, this system
8 exhibits higher n_s values, an artifact of the increased active site density of some of the
9 particles. While this data is retrieved with a cold plate, it falls within the range of the
10 aerosolized methods where particle surface areas are small. Finally, more of the
11 suspension method range of retrieved n_s can be spanned by data where the concentration
12 saturation effect takes place. Data that exhibited this behavior from the CMU cold plate
13 system (golden triangles) and the Broadley et al. system (red and brown bowties) are
14 plotted. This effect tends to underestimate n_s since additional material is added while the
15 freezing behavior remains the same. Thus just by varying particle concentration and
16 surface area of illite in the droplets, cold plate measurements can span the range of n_s
17 values obtained by the various aerosol and wet suspension measurement methods. We
18 emphasize again that $n_s(T)$ should be the same for the same system, and this metric is
19 often used as the major means to compare and evaluate different INP measurement
20 methods.

21 Various research groups using wet suspension methods typically vary particle
22 concentrations to span a wider range of measureable droplet freezing temperature
23 (Broadley et al., 2012; Murray et al., 2012; Wright and Petters, 2013). Our analysis
24 indicates that by doing so different n_s values are in fact retrieved, just due to changes in
25 concentration. This highlights the importance of obtaining n_s values that overlap in
26 temperature space, to evaluate if n_s is in fact consistent as concentration is changed. We
27 therefore provide the critical area framework presented here whereby ice nucleating
28 surface area dependence is more complex than depicted in traditional deterministic and
29 stochastic models, as a potential source of the discrepancy in n_s values for the various
30 measurement techniques. This commonly observed discrepancy in n_s between droplet
31 suspension and aerosol INP measurement methods is the subject of ongoing

Deleted: gold and green rectangles).

Deleted: purple hexagons

1 investigations, such as the INUIT project that is currently focusing on cellulose particles,
 2 a system we have included here. As the results from this multi-investigator project have
 3 not yet been published we cannot present them here. They show a similar trend as for the
 4 illite NX data, where the aerosol methods retrieve higher n_s values than the droplet
 5 suspension methods do. By changing particle in droplet concentration we can span much
 6 of the difference in n_s between the two groups of methods, as was shown for the illite NX
 7 measurements.

8 **4 Application of the g parameterization to cloud models**

9 Particle type-specific \bar{g} distributions and critical areas can be used in larger cloud and
 10 atmospheric models to predict freezing onset and the rate of continued ice formation. The
 11 simplest parameterization is one that calculates the frozen fraction of droplets, F , for an
 12 atmospherically realistic system in which one ice nucleating particle is present in each
 13 supercooled droplet, the aerosol particle distribution is monodisperse (all particles
 14 therefore have the same surface area A), there is only one species present (therefore one \bar{g}
 15 distribution is used), and the surface area of the individual particles is larger than that
 16 species' critical area. In this case Eq. (15) can be used:

$$17 \quad F = 1 - \exp\left(-tA \int_0^\pi J(\theta, T) \overline{g(\theta)} d\theta\right) \quad (15)$$

18 If the surface area of the individual particles is smaller than the critical area a modified
 19 version of Eq. (19) can be used instead:

$$20 \quad F = 1 - \exp\left(-tA_c \int_0^\pi (J(\theta, T) \overline{g(\theta)} d\theta) h(A, T)\right) \quad (19)$$

21 where $h(A, T)$ is an empirically derived parameterization that corrects for the individual
 22 particle surface areas of the considered monodisperse aerosol population being smaller
 23 than the critical area. Therefore $h(A_c, T) = 1$.

24 An example of retrieving values of $h(A, T)$ would be in correcting the solid line for
 25 system 4a ($7.11 \times 10^{-6} \text{ cm}^2$) to the dotted line in Fig. 5. The solid line is the basic use of
 26 Eq. (15) however it was shown that the considered experimentally retrieved freezing

1 spectrum was below the critical area threshold. By taking the ratio of the dotted and solid
 2 lines values of h can be retrieved for that surface area at each temperature point.

3 If the aerosol particle population is polydisperse and its size distribution can be
 4 expressed as a function of surface area, the frozen fraction can be written as:

$$5 \quad F = \int_{A_i}^{A_f} \left[1 - \exp \left(-tA \int_0^\pi (J(\theta, T) \bar{g}(\theta) d\theta) h(A, T) dA \right) \right] \quad (20)$$

6 where A_i and A_f are the minimum and maximum values of the surface areas of the
 7 aerosol particle distribution.

8 If the aerosol ice nucleating population is composed of multiple species, two \bar{g}
 9 parameterizations can be formulated for the two cases of an internally mixed (every
 10 particle is composed of all the different species) and externally mixed (every particle is
 11 composed of just one species). For the case of an internally mixed system Eqs. (15), (19),
 12 and (20) can be applied with a \bar{g} distribution that is the surface area weighted average of
 13 the \bar{g} distributions of all the considered species. This can be expressed as:

$$17 \quad \bar{g}_{average} = \frac{1}{A} \sum_{i=1}^m A_i \bar{g}_i \quad (21)$$

14 where A_i is the surface area of the species i , \bar{g}_i is the \bar{g} distribution of the species i , and m
 15 is the total number of species. If the system is externally mixed, the frozen fraction can be
 16 expressed as:

$$18 \quad F = \frac{1}{m} \sum_{i=1}^m F_i \quad (22)$$

19 where F_i is the frozen fraction of droplets containing particles of species i and can be
 20 retrieved from Eq. (19) or (20).

21

22 **5 Conclusions**

23 Cold plate droplet freezing spectra were carefully examined to investigate a surface
 24 area dependence of ice nucleation ability whereby one active site density function such as

1 n_s cannot be extrapolated from high particle surface area to low particle surface area
2 conditions. A method based on the notion of a critical surface area threshold was
3 presented. It is argued that a species' entire ice nucleating spectrum can be confined
4 within a global probability density function \bar{g} . For a system, be it one particle or an
5 ensemble of particles, to have a total surface area greater than the critical area is a
6 question of whether the surface is large enough to express all the variability in that
7 particle species' ice active surface site ability. By analyzing droplets containing illite
8 minerals, MCC cellulose, and commercial Snomax bacterial particles, it was shown that
9 freezing curves above a certain critical surface area threshold could be predicted directly
10 from the global \bar{g} distribution obtained from the high particle concentration data alone.
11 The lower particle concentration freezing curves were accurately predicted by randomly
12 sampling active site abilities (θ) from \bar{g} and averaging their resultant freezing
13 probabilities. This framework provides a new method for extrapolating droplet freezing
14 temperature spectra from cold plate experimental data under high particle concentrations
15 to atmospherically realistic dilute particle-droplet systems.

16 We found that the shifts to colder freezing temperatures caused by reducing the
17 particle concentration or total surface area present in droplets cannot be fully accounted
18 for by simply normalizing to the available surface area, as is done in the ice active site
19 density (n_s) analysis framework. When the surface area is below the critical area
20 threshold the retrieved values of n_s can increase significantly for the same particle species
21 when the particle concentration is decreased. Above the critical area threshold the same n_s
22 curves are retrieved when particle concentration is changed. Atmospheric cloud droplets
23 typically contain just one particle each. Therefore, this effect of particle concentration on
24 droplet freezing temperature spectra and the retrieved n_s values has important
25 implications for the extrapolation of cold plate droplet freezing measurements to describe
26 the ice nucleation properties of realistic atmospheric particles.

27 Systems that probe populations of droplets each containing one particle such as the
28 CFDC are unable to probe a large particles-in-droplet concentration range but are
29 powerful tools for the real-time investigations of ice nucleating particles at the realistic
30 individual particle level (DeMott et al., 2010; Sullivan et al., 2010a; Welti et al., 2009).

1 The frozen fraction curves produced from such an instrument do not provide enough
2 information to associate the observed variability in ice nucleation ability to internal or
3 external factors. However, future laboratory studies using the critical area-cold plate
4 technique we have introduced here (e.g. Fig. 4) will provide new insight into the critical
5 area thresholds of internal variability in ice active site ability for different species. This
6 will produce more informed assumptions regarding the variability in ice nucleation
7 properties observed through online field instruments, specifically when the measurements
8 are made in conjunction with single particle chemical analysis techniques (Creamean et
9 al., 2013; DeMott et al., 2003, 2010; Prather et al., 2013; Worringer et al., 2015).

10 Atmospherically relevant particle sizes may very well fall below the critical area
11 threshold for an individual particle, at least for some species such as illite mineral
12 particles considered here. Therefore, average ice nucleation spectra or active site
13 distributions such as n_s and \bar{g} may not be applicable for representing the ice nucleation
14 properties of particles in cloud and atmospheric models. However careful examination of
15 the surface area dependence of ice nucleating ability of a species allows more accurate
16 retrievals of active site density distributions that properly encompass this dependence.

17

18 Acknowledgements

19 This research was partially supported by the National Science Foundation (Award
20 CHE-1213718), and M.P. was supported by a NSF Graduate Research Fellowship. The
21 authors thank Dr. Paul DeMott for valuable discussions regarding an earlier version of
22 this framework. Dr. Naruki Hiranuma at AIDA is acknowledged for providing us with
23 the MCC cellulose and illite NX samples, as part of the INUIT project.

24

25 6 References

26 Alpert, P. A. and Knopf, D. A.: Analysis of isothermal and cooling-rate-dependent
27 immersion freezing by a unifying stochastic ice nucleation model, Atmos. Chem. Phys.,
28 16(4), 2083–2107, doi:10.5194/acp-16-2083-2016, 2016.

29 Andreae, M. O. and Rosenfeld, D.: Aerosol–cloud–precipitation interactions. Part 1.
30 The nature and sources of cloud-active aerosols, Earth-Science Rev., 89(1–2), 13–41,
31 doi:10.1016/j.earscirev.2008.03.001, 2008.

Deleted: .

Deleted: sample

Formatted: Line spacing: single

Deleted: -

- | 1 Baker, M. B. and Peter, T.: Small-scale cloud processes and climate., *Nature*,
2 451(7176), 299–300, doi:10.1038/nature06594, 2008.
- | 3 Barahona, D.: On the ice nucleation spectrum, *Atmos. Chem. Phys.*, 12(8), 3733–
4 3752, 2012.
- | 5 Broadley, S. L., Murray, B. J., Herbert, R. J., Atkinson, J. D., Dobbie, S., Malkin, T.
6 L., Condcliffe, E. and Neve, L.: Immersion mode heterogeneous ice nucleation by an illite
7 rich powder representative of atmospheric mineral dust, *Atmos. Chem. Phys.*, 12, 287–
8 307, doi:10.5194/acp-12-287-2012, 2012.
- | 9 Cantrell, W. and Heymsfield, A.: Production of Ice in Tropospheric Clouds: A
10 Review, *Bull. Am. Meteorol. Soc.*, 86(6), 795–807, doi:10.1175/BAMS-86-6-795, 2005.
- | 11 Creamean, J. M., Suski, K. J., Rosenfeld, D., Cazorla, A., DeMott, P. J., Sullivan, R.
12 C., White, A. B., Ralph, F. M., Minnis, P., Comstock, J. M., Tomlinson, J. M. and
13 Prather, K. a: Dust and biological aerosols from the Sahara and Asia influence
14 precipitation in the western U.S., *Science*, 339(6127), 1572–8,
15 doi:10.1126/science.1227279, 2013.
- | 16 DeMott, P. J., Cziczo, D. J., Prenni, A. J., Murphy, D. M., Kreidenweis, S. M.,
17 Thomson, D. S., Borys, R. and Rogers, D. C.: Measurements of the concentration and
18 composition of nuclei for cirrus formation., *Proc. Natl. Acad. Sci. U. S. A.*, 100(25),
19 14655–60, doi:10.1073/pnas.2532677100, 2003.
- | 20 DeMott, P. J., Prenni, A. J., Liu, X., Kreidenweis, S. M., Petters, M. D., Twohy, C. H.
21 and Richardson, M. S.: Predicting global atmospheric ice nuclei distributions and their
22 impacts on climate, *PNAS*, 107(25), 11217–11222, doi:10.1073/pnas.0910818107, 2010.
- | 23 Eidhammer, T., DeMott, P. J. and Kreidenweis, S. M.: A comparison of heterogeneous
24 ice nucleation parameterizations using a parcel model framework, *J. Geophys. Res.*, 114,
25 D06202, doi:10.1029/2008jd011095, 2009.
- | 26 Emersic, C., Connolly, P. J., Boulton, S., Campana, M. and Li, Z.: Investigating the
27 discrepancy between wet suspension and dry-dispersion derived ice nucleation efficiency
28 of mineral particles, *Atmos. Chem. Phys.*, 15(19), 11311–11326, doi:10.5194/acp-15-
29 11311-2015, 2015.
- | 30 Ervens, B. and Feingold, G.: On the representation of immersion and condensation
31 freezing in cloud models using different nucleation schemes, *Atmos. Chem. Phys.*, 12,
32 5807–5826, doi:10.5194/acp-12-5807-2012, 2012.
- | 33 Ervens, B. and Feingold, G.: Sensitivities of immersion freezing: Reconciling classical
34 nucleation theory and deterministic expressions, *Geophys. Res. Lett.*, 40(April), 3320–
35 3324, doi:10.1002/grl.50580, 2013.
- | 36 Ervens, B., Feingold, G., Sulia, K. and Harrington, J.: The impact of microphysical
37 parameters, ice nucleation mode, and habit growth on the ice/liquid partitioning in mixed-
38 phase Arctic clouds, *J. Geophys. Res.*, 116(D17), D17205, doi:10.1029/2011JD015729,
39 2011.
- | 40 Fletcher, N. H.: Active Sites and Ice Crystal Nucleation, *J. Atmos. Sci.*, 26(6), 1266–

- 1 1271, doi:10.1175/1520-0469(1969)026<1266:ASAICN>2.0.CO;2, 1969.
- 2 Fornea, A. P., Brooks, S. D., Dooley, J. B. and Saha, A.: Heterogeneous freezing of
3 ice on atmospheric aerosols containing ash, soot, and soil, *J. Geophys. Res.*, 114(D13),
4 D13201, doi:10.1029/2009JD011958, 2009.
- 5 [Hartmann, S., Wex, H., Clauss, T., Augustin-Bauditz, S., Niedermeier, D., Rösch, M.
6 and Stratmann, F.: Immersion Freezing of Kaolinite: Scaling with Particle Surface Area,
7 *J. Atmos. Sci.*, 73\(1\), 263–278 \[online\] Available from:
8 <http://journals.ametsoc.org/doi/abs/10.1175/JAS-D-15-0057.1>, 2016.](#)
- 9 [Herbert, R. J., Murray, B. J., Whale, T. F., Dobbie, S. J. and Atkinson, J. D.:
10 Representing time-dependent freezing behaviour in immersion mode ice nucleation,
11 *Atmos. Chem. Phys.*, 14\(16\), 8501–8520, 2014.](#)
- 12 Hiranuma, N., Augustin-Bauditz, S., Bingemer, H., Budke, C., Curtius, J., Danielczok,
13 A., Diehl, K., Dreischmeier, K., Ebert, M., Frank, F., Hoffmann, N., Kandler, K.,
14 Kiselev, A., Koop, T., Leisner, T., Möhler, O., Nillius, B., Peckhaus, A., Rose, D.,
15 Weinbruch, S., Wex, H., Boose, Y., DeMott, P. J., Hader, J. D., Hill, T. C. J., Kanji, Z.
16 A., Kulkarni, G., Levin, E. J. T., McCluskey, C. S., Murakami, M., Murray, B. J.,
17 Niedermeier, D., Petters, M. D., O’Sullivan, D., Saito, A., Schill, G. P., Tajiri, T.,
18 Tolbert, M. A., Welti, A., Whale, T. F., Wright, T. P. and Yamashita, K.: A
19 comprehensive laboratory study on the immersion freezing behavior of illite NX
20 particles: a comparison of 17 ice nucleation measurement techniques, *Atmos. Chem.
21 Phys.*, 15(5), 2489–2518, doi:10.5194/acp-15-2489-2015, 2015a.
- 22 Hiranuma, N., Möhler, O., Yamashita, K., Tajiri, T., Saito, A., Kiselev, A., Hoffmann,
23 N., Hoose, C., Jantsch, E., Koop, T. and Murakami, M.: Ice nucleation by cellulose and
24 its potential contribution to ice formation in clouds, *Nat. Geosci.*, 8(4), 273–277,
25 doi:10.1038/ngeo2374, 2015b.
- 26 Hoose, C. and Möhler, O.: Heterogeneous ice nucleation on atmospheric aerosols: A
27 review of results from laboratory experiments, *Atmos. Chem. Phys.*, 12(20), 9817–9854,
28 2012.
- 29 Hoose, C., Lohmann, U., Erdin, R. and Tegen, I.: The global influence of dust
30 mineralogical composition on heterogeneous ice nucleation in mixed-phase clouds,
31 *Environ. Res. Lett.*, 3(2), ~~25003~~, doi:10.1088/1748-9326/3/2/025003, 2008.
- 32 Hoose, C., Kristjánsson, J. E., Chen, J.-P. and Hazra, A.: A Classical-Theory-Based
33 Parameterization of Heterogeneous Ice Nucleation by Mineral Dust, Soot, and Biological
34 Particles in a Global Climate Model, *J. Atmos. Sci.*, 67(8), 2483–2503, 2010.
- 35 Koehler, K. a., Kreidenweis, S. M., DeMott, P. J., Petters, M. D., Prenni, a. J. and
36 Möhler, O.: Laboratory investigations of the impact of mineral dust aerosol on cold cloud
37 formation, *Atmos. Chem. Phys.*, 10(23), 11955–11968, doi:10.5194/acp-10-11955-2010,
38 2010.
- 39 Koop, T., Luo, B., Tsias, a and Peter, T.: Water activity as the determinant for
40 homogeneous ice nucleation in aqueous solutions, *Nature*, 406(6796), 611–4,
41 doi:10.1038/35020537, 2000.

Formatted: Line spacing: single

Deleted: 025003

- 1 Levine, J.: Statistical explanation of spontaneous freezing of water droplets, NACA
2 Tech. (Note), 2234, 1950.
- 3 Liu, X. and Penner, J. E.: Ice nucleation parameterization for global models, Meteorol.
4 Zeitschrift, 14(4), 499–514, 2005.
- 5 Lüönd, F., Stetzer, O., Welti, A. and Lohmann, U.: Experimental study on the ice
6 nucleation ability of size-selected kaolinite particles in the immersion mode, J. Geophys.
7 Res., 115(D14), D14201, doi:10.1029/2009JD012959, 2010.
- 8 Marcolli, C., Gedamke, S., Peter, T. and Zobrist, B.: Efficiency of immersion mode
9 ice nucleation on surrogates of mineral dust, Atmos. Chem. Phys., 7(19), 5081–5091,
10 2007.
- 11 Meyers, M. P., DeMott, P. J. and Cotton, W. R.: New Primary Ice-Nucleation
12 Parameterizations in an Explicit Cloud Model, J. Appl. Meteorol., 31(7), 708–721,
13 doi:10.1175/1520-0450(1992)031<0708:NPINPI>2.0.CO;2, 1992.
- 14 Mülmstädt, J., Sourdeval, O., Delanoë, J. and Quaas, J.: Frequency of occurrence of
15 rain from liquid-, mixed-, and ice-phase clouds derived from A-Train satellite retrievals,
16 Geophys. Res. Lett., 42(15), 6502–6509, doi:10.1002/2015GL064604, 2015.
- 17 Murray, B. J., Broadley, S. L., Wilson, T. W., Atkinson, J. D. and Wills, R. H.:
18 Heterogeneous freezing of water droplets containing kaolinite particles, Atmos. Chem.
19 Phys., 11(9), 4191–4207, 2011.
- 20 Murray, B. J., O’Sullivan, D., Atkinson, J. D. and Webb, M. E.: Ice nucleation by
21 particles immersed in supercooled cloud droplets, Chem. Soc. Rev., 41(19), 6519,
22 doi:10.1039/c2cs35200a, 2012.
- 23 Niedermeier, D., Shaw, R. a., Hartmann, S., Wex, H., Clauss, T., Voigtländer, J. and
24 Stratmann, F.: Heterogeneous ice nucleation: exploring the transition from stochastic to
25 singular freezing behavior, Atmos. Chem. Phys., 11(16), 8767–8775, doi:10.5194/acp-
26 11-8767-2011, 2011.
- 27 [Pandey, R., Usui, K., Livingstone, R. A., Fischer, S. A., Pfaendtner, J., Backus, E. H.,
28 G., Nagata, Y., Fröhlich-nowoisky, J., Schmäser, L., Mauri, S., Scheel, J. F., Knopf, D.,
29 A., Pöschl, U., Bonn, M. and Weidner, T.: Ice-nucleating bacteria control the order and
30 dynamics of interfacial water, Sci. Adv., 2\(4\), 1–9, doi:10.1126/sciadv.1501630, 2016.](#)
- 31 Phillips, V. T. J., DeMott, P. J. and Andronache, C.: An Empirical Parameterization of
32 Heterogeneous Ice Nucleation for Multiple Chemical Species of Aerosol, J. Atmos. Sci.,
33 65(9), 2757–2783, doi:10.1175/2007JAS2546.1, 2008.
- 34 Phillips, V. T. J., Demott, P. J., Andronache, C., Pratt, K. A., Prather, K. A.,
35 Subramanian, R. and Twohy, C.: Improvements to an Empirical Parameterization of
36 Heterogeneous Ice Nucleation and its Comparison with Observations, J. Atmos. Sci.,
37 120927133920007, 2012.
- 38 Polen, M., Lawlis, E. and Sullivan, R. C.: The unstable ice nucleation properties of
39 Snomax(R) bacterial particles, J. Geophys. Res. - Atmos., [Accepted](#), 2016.
- 40 Prather, K. a, Bertram, T. H., Grassian, V. H., Deane, G. B., Stokes, M. D., Demott, P.

Formatted: Line spacing: single

Deleted: Submitted

- 1 J., Aluwihare, L. I., Palenik, B. P., Azam, F., Seinfeld, J. H., Moffet, R. C., Molina, M. J.,
2 Cappa, C. D., Geiger, F. M., Roberts, G. C., Russell, L. M., Ault, A. P., Baltrusaitis, J.,
3 Collins, D. B., Corrigan, C. E., Cuadra-Rodriguez, L. a, Ebben, C. J., Forestieri, S. D.,
4 Guasco, T. L., Hersey, S. P., Kim, M. J., Lambert, W. F., Modini, R. L., Mui, W., Pedler,
5 B. E., Ruppel, M. J., Ryder, O. S., Schoepp, N. G., Sullivan, R. C. and Zhao, D.:
6 Bringing the ocean into the laboratory to probe the chemical complexity of sea spray
7 aerosol., *Proc. Natl. Acad. Sci. U. S. A.*, 110(19), 7550–5, doi:10.1073/pnas.1300262110,
8 2013.
- 9 Pruppacher, H. R. and Klett, J. D.: *Microphysics of Clouds and Precipitation*, edited
10 by R. D. Rosen, Kluwer Academic Publishers., 1997.
- 11 Rosenfeld, D., Lohmann, U., Raga, G. B., O’Dowd, C. D., Kulmala, M., Fuzzi, S.,
12 Reissell, A. and Andreae, M. O.: Flood or Drought: How Do Aerosols Affect
13 Precipitation?, *Science* (80-.), 321(5894), 1309–1313, doi:10.1126/science.1160606,
14 2008.
- 15 Sear, R. P.: Generalisation of Levine ’ s prediction for the distribution of freezing
16 temperatures of droplets : a general singular model for ice nucleation, *Atmos. Chem.*
17 *Phys.*, 13, 7215–7223, doi:10.5194/acp-13-7215-2013, 2013.
- 18 Sullivan, R. C., Miñambres, L., DeMott, P. J., Prenni, A. J., Carrico, C. M., Levin, E.
19 J. T. and Kreidenweis, S. M.: Chemical processing does not always impair heterogeneous
20 ice nucleation of mineral dust particles, *Geophys. Res. Lett.*, 37(24),
21 doi:10.1029/2010GL045540, 2010a.
- 22 Sullivan, R. C., Petters, M. D., DeMott, P. J., Kreidenweis, S. M., Wex, H.,
23 Niedermeier, D., Hartmann, S., Clauss, T., Stratmann, F., Reitz, P., Schneider, J. and
24 Sierau, B.: Irreversible loss of ice nucleation active sites in mineral dust particles caused
25 by sulphuric acid condensation, *Atmos. Chem. Phys.*, 10(23), 11471–11487, 2010b.
- 26 [Turner, M. A., Arellano, F. and Kozloff, L. M.: Three separate classes of bacterial ice
27 nucleation structures, *J. Bacteriol.*, 172\(5\), 2521–2526, 1990.](#)
- 28 Vali, G.: Quantitative Evaluation of Experimental Results an the Heterogeneous
29 Freezing Nucleation of Supercooled Liquids, *J. Atmos. Sci.*, 28(3), 402–409,
30 doi:10.1175/1520-0469(1971)028<0402:QEOERA>2.0.CO;2, 1971.
- 31 Vali, G.: Freezing Rate Due to Heterogeneous Nucleation, *J. Atmos. Sci.*, 51(13),
32 1843–1856, doi:10.1175/1520-0469(1994)051<1843:FRDTHN>2.0.CO;2, 1994.
- 33 Vali, G.: Repeatability and randomness in heterogeneous freezing nucleation, *Atmos.*
34 *Chem. Phys.*, 8(16), 5017–5031, doi:10.5194/acp-8-5017-2008, 2008.
- 35 Vali, G.: Interpretation of freezing nucleation experiments: Singular and stochastic;
36 Sites and surfaces, *Atmos. Chem. Phys.*, 14(11), 5271–5294, 2014.
- 37 Vali, G. and Snider, J. R.: [Time-dependent freezing rate parcel model, *Atmos. Chem.*
38 *Phys.*, 15\(4\), 2071–2079, doi:10.5194/acp-15-2071-2015, 2015.](#)
- 39 [Vali, G. and Stransbury, E. J.: Time Dependant Charactirisits of the Heterogeneous
40 Nucleation of Ice, *Can. J. Phys.*, 44\(3\), 477–502, 1966.](#)

Formatted: Line spacing: single

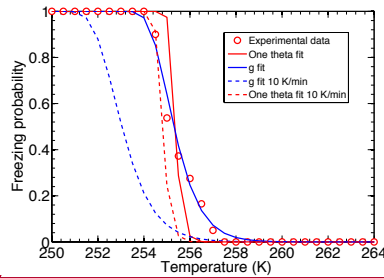
Formatted: Line spacing: single

- 1 Vali, G., DeMott, P. J., Möhler, O. and Whale, T. F.: Technical Note: A proposal for
2 ice nucleation terminology, *Atmos. Chem. Phys.*, 15(18), 10263–10270, doi:10.5194/acp-
3 15-10263-2015, 2015.
- 4 Welti, A., Lund, F., Stetzer, O. and Lohmann, U.: Influence of particle size on the ice
5 nucleating ability of mineral dusts, *Atmos. Chem. Phys.*, 9(18), 6705–6715, 2009.
- 6 Welti, A., Lüönd, F., Kanji, Z. A., Stetzer, O. and Lohmann, U.: Time dependence of
7 immersion freezing: an experimental study on size selected kaolinite particles, *Atmos.*
8 *Chem. Phys.*, 12(20), 9893–9907, doi:10.5194/acp-12-9893-2012, 2012.
- 9 Wex, H., Augustin-Bauditz, S., Boose, Y., Budke, C., Curtius, J., Diehl, K., Dreyer,
10 a., Frank, F., Hartmann, S., Hiranuma, N., Jantsch, E., Kanji, Z. a., Kiselev, a., Koop, T.,
11 Möhler, O., Niedermeier, D., Nillius, B., Rösch, M., Rose, D., Schmidt, C., Steinke, I.
12 and Stratmann, F.: Intercomparing different devices for the investigation of ice nucleating
13 particles using Snomax® as test substance, *Atmos. Chem. Phys.*, 15(3), 1463–1485,
14 doi:10.5194/acp-15-1463-2015, 2015.
- 15 Wheeler, M. J. and Bertram, A. K.: Deposition nucleation on mineral dust particles: A
16 case against classical nucleation theory with the assumption of a single contact angle,
17 *Atmos. Chem. Phys.*, 12(2), 1189–1201, doi:10.5194/acp-12-1189-2012, 2012.
- 18 Worrigen, a., Kandler, K., Benker, N., Dirsch, T., Mertes, S., Schenk, L., Kästner,
19 U., Frank, F., Nillius, B., Bundke, U., Rose, D., Curtius, J., Kupiszewski, P.,
20 Weingartner, E., Vochezer, P., Schneider, J., Schmidt, S., Weinbruch, S. and Ebert, M.:
21 Single-particle characterization of ice-nucleating particles and ice particle residuals
22 sampled by three different techniques, *Atmos. Chem. Phys.*, 15(8), 4161–4178,
23 doi:10.5194/acp-15-4161-2015, 2015.
- 24 Wright, T. P. and Petters, M. D.: The role of time in heterogeneous freezing
25 nucleation, *J. Geophys. Res. Atmos.*, 118(9), 3731–3743, 2013.
- 26 Wright, T. P., Petters, M. D., Hader, J. D., Morton, T. and Holder, A. L.: Minimal
27 cooling rate dependence of ice nuclei activity in the immersion mode, *J. Geophys. Res.*
28 *Atmos.*, 118(18), 10,535–10,543, doi:10.1002/jgrd.50810, 2013.
- 29 [Yankofsky, S. a., Levin, Z., Bertold, T. and Sandlerman, N.: Some Basic](#)
30 [Characteristics of Bacterial Freezing Nuclei, *J. Appl. Meteorol.*, 20\(9\), 1013–1019,](#)
31 [doi:10.1175/1520-0450\(1981\)020<1013:SBCOBF>2.0.CO;2, 1981.](#)
- 32 Zobrist, B., Koop, T., Luo, B. P., Marcolli, C. and Peter, T.: Heterogeneous ice
33 nucleation rate coefficient of water droplets coated by a nonadecanol monolayer, *J. Phys.*
34 *Chem. C*, 111(1), 2149–2155, doi:10.1021/jp066080w, 2007.

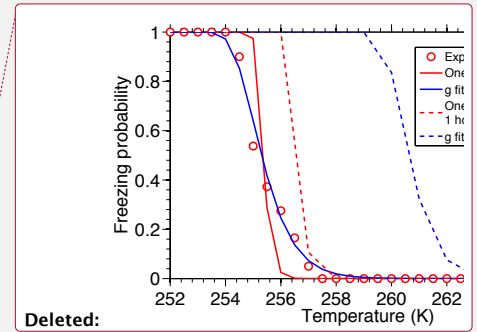
Deleted: –

Formatted: Line spacing: single

35
36



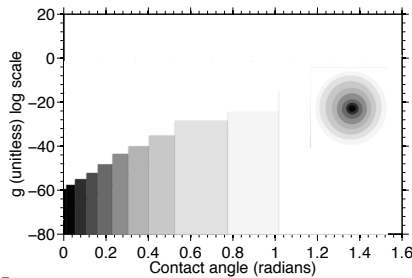
1
2
3 **Figure 1.** Experimentally determined freezing probabilities and fits from freezing of a
4 droplet containing a single large $\sim 300 \mu\text{m}$ diameter volcanic ash particle, from Fornea et
5 al. (2009). Red dots are experimental freezing probabilities retrieved from repeated
6 droplet freezing measurements. The red line is a fit to the data using classical nucleation
7 theory and the assumption of a single contact angle (θ). The blue line is a fit to the data
8 using the g framework developed here, which describes a Gaussian distribution of θ . The
9 g fit has a least square error sum of 0.0197, $\mu = 1.65$, and $\sigma = 0.135$. The dotted red line
10 is the simulated freezing curve resulting from a single θ distribution for a simulated
11 cooling rate of 10 K/min. The dotted blue line is the freezing curve from a multiple θ
12 distribution described by g after the same simulated cooling rate.



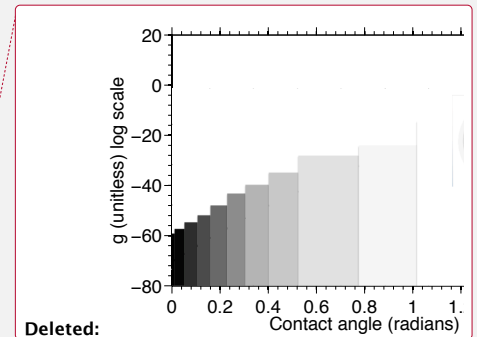
Deleted:

Deleted: after the droplets are held at the same temperature for 1 hour.

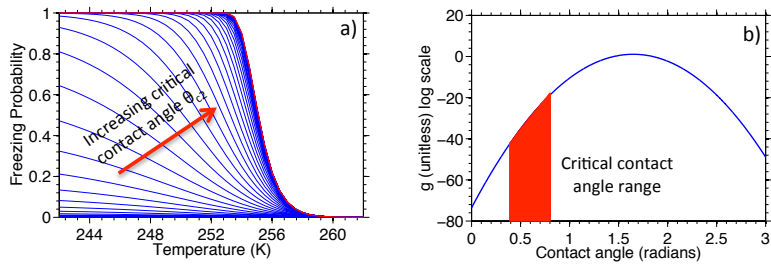
Deleted: temperature hold simulation



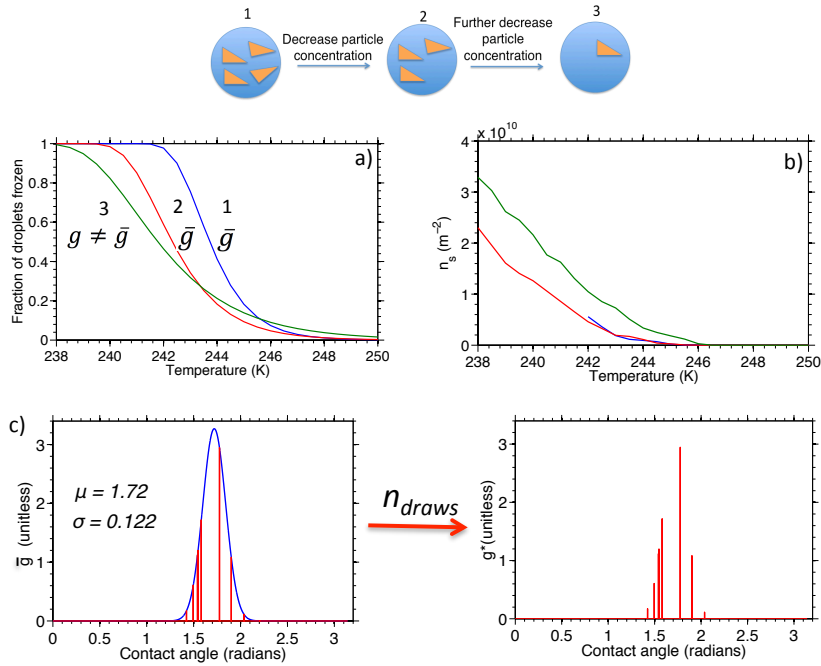
16
17
18 **Figure 2.** Upper right inset displays the distribution of ice nucleation activity (contact
19 angle, θ) for a representative spectrum of a particle's ice nucleating activity. The less
20 active (white) surface sites have more surface coverage while the more active (black)
21 surface sites have less coverage. The probability distribution function for the g
22 distribution ($\mu = 1.65$, and $\sigma = 0.135$, retrieved in Section 3.1) ascent in log space is
23 plotted with numerical bins. The darker colors are used to highlight the stronger ice
24 nucleating activity at smaller contact angles (θ).



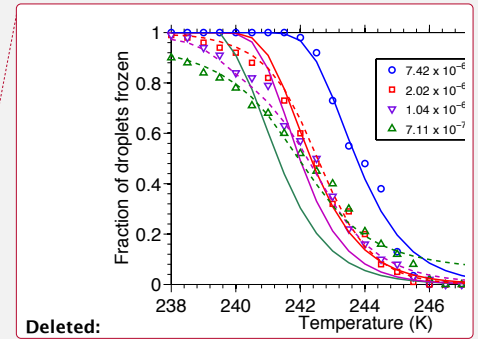
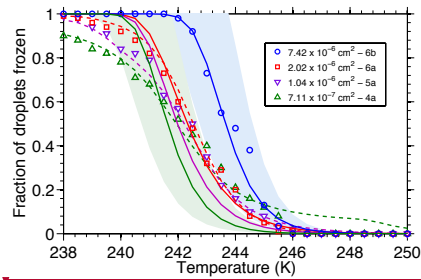
Deleted:



1
2
3 **Figure 3. Left (a):** Identifying the critical contact angle range. The thin blue curves are
4 retrieved from application of the simplified Eq. (10), which approximates the freezing
5 probability by integrating over a smaller contact angle range, $[\theta_{c1}, \theta_{c2}]$, while the thick
6 red curve is obtained from application of the complete Eq. (7), which integrates over the
7 full contact angle range. Both approaches use the same g distribution retrieved for the
8 case example in section 3.1 with $\mu = 1.65$, and $\sigma = 0.135$. **Right (b):** The g distribution
9 from the case example in Section 3.1 plotted in log scale and showing the critical contact
10 angle range retrieved in Section 3.2 ($\theta_{c1} \approx 0.4$ rad and $\theta_{c2} \approx 0.79$) in red.
11
12



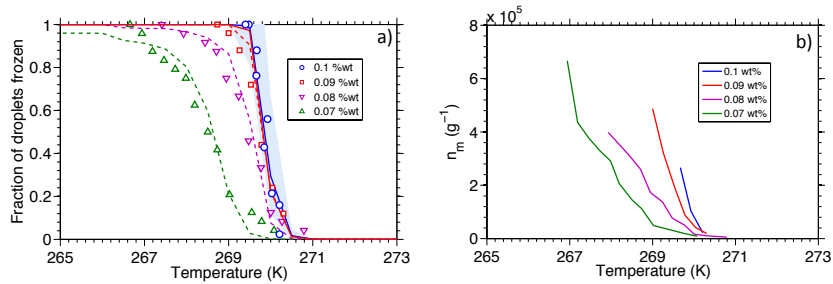
1
2
3
4 **Figure 4. Top:** Schematic summarizing the procedure for determining the critical area.
5 **Left (a):** The frozen fraction freezing curves shift to lower temperatures initially due to
6 solely to the decrease in total surface area of the ice nucleating particles (curves 1 & 2).
7 As the total surface area of the particles is decreased below the critical area threshold
8 ($g \neq \bar{g}$) the slope of the freezing curve also broadens because the effective distribution
9 of ice nucleating sites has changed – more external variability has been introduced (curve
10 3). **Right (b):** Ice active site density (n_s) retrieved from the frozen fraction plots on the
11 left for the same three particle concentration systems. Above the critical area limit ($g =$
12 \bar{g}) the two n_s curves are essentially the same, but below the critical area threshold ($g \neq$
13 \bar{g}) n_s increases, even though the same particle species was measured in all three
14 experiments. These exemplary frozen fraction and n_s curves were produced by fitting a \bar{g}
15 distribution to droplet freezing measurements of illite mineral particles from Broadley et
16 al. (2012). **Bottom (c):** Schematic summarizing how g^* is retrieved from \bar{g} using n_{draws} . In
17 each draw a random contact angle from the full range of contact angles $[0, \pi]$ is chosen
18 after which the value of g^* at that contact angle (right) is assigned the value of \bar{g} at the
19 same contact angle (left).
20



Deleted:

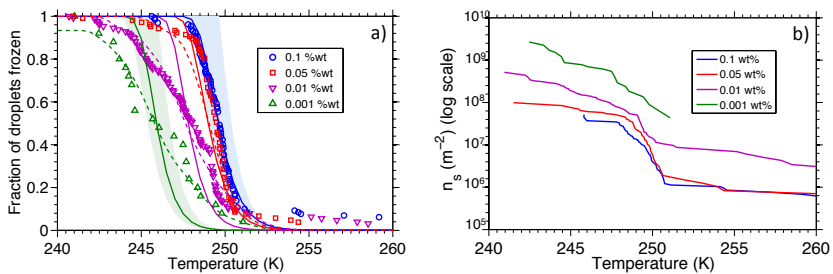
Deleted: .

1
2
3 **Figure 5.** Experimental freezing curves for different surface area concentrations of illite
4 mineral powder immersed in 10-20 μm diameter water droplets taken from Broadley et
5 al. (2012) (circles). Lines are modeled predictions of the same data using the g^*
6 distribution method. Solid lines are produced directly from the global \bar{g} distribution first
7 obtained from the high concentration system. The dashed lines are obtained by randomly
8 sub-sampling the global \bar{g} distribution to obtain g^* and following a surface area
9 correction, as described in the text. The shaded region shows the predicted temperature
10 range over which freezing of droplets occurs for the surface area variability associated
11 with the droplet diameter range of 10-20 μm using \bar{g} (i.e. running Eq. (9) with different
12 values for A), for the highest and lowest particle concentration experiments.
13
14



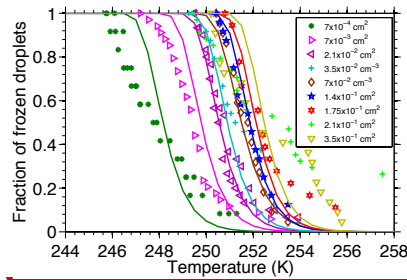
1
2
3 **Figure 6. Left (a):** Experimental freezing curves for different mass concentrations of
4 commercial Snomax powder immersed in 500-700 μm diameter water droplets obtained
5 using the CMU cold plate (circles). Solid lines are fits produced from randomly sampling
6 from the \bar{g} distribution retrieved from the highest concentration freezing curve (0.1 %wt).
7 Dashed lines are fits produced from randomly sampling from the \bar{g} distribution and a
8 surface area correction. The second highest concentration freezing curve (0.09 %wt) is
9 used to confirm the critical area threshold had been exceeded. The shaded region
10 represents the effect of variability in surface area as in Fig. 5 but for a droplet diameter
11 range of 500-700 μm , for the highest particle concentration. **Right (b):** Ice active site
12 density (n_m) retrieved from the frozen fraction data on the left. A trend of decreasing n_m
13 with decreasing concentration is observed for the droplets containing Snomax.

Formatted: Font:Not Bold
Formatted: Centered, Indent: Left: -0.44", First line: 0.2"
Deleted: 200-300



16
17
18 **Figure 7. Left (a):** Experimental freezing curves for different mass concentrations of
19 MCC cellulose powder immersed in 500-700 μm diameter water droplets obtained
20 using the CMU cold plate (circles). Dashed lines are fits produced from randomly sampling
21 from the \bar{g} distribution retrieved from the highest concentration freezing curve (0.1 wt%,
22 blue solid line) and a surface area correction. The second highest concentration freezing
23 curve (0.05 wt%, red) is used to confirm the critical area threshold was exceeded. The
24 shaded region represents the effect of variability in surface area as in Fig. 5 but for a
25 droplet diameter range of 500-700 μm , for the highest and lowest particle concentration
26 experiments. **Right (b):** Ice active site density (n_s) retrieved from the frozen fraction data
27 on the left. A trend of increasing n_s with decreasing concentration is observed.

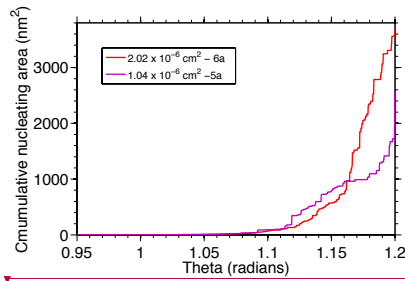
Formatted: Justified, Indent: First line: 0"
Deleted:
Deleted: 600
Formatted: Font:Not Bold



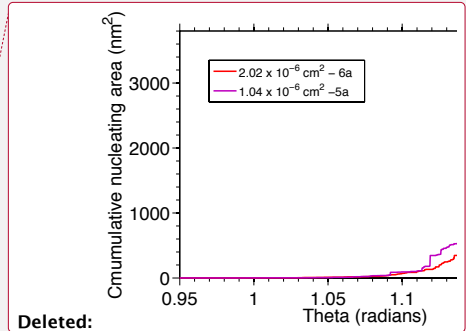
Deleted: ... [1]

1
2
3 **Figure 8.** Experimental freezing curves for different mass concentrations of illite NX
4 powder immersed in 500-700 μm diameter water droplets obtained using the CMU cold
5 plate (circles). The solid lines are the predicted frozen fractions based on the \bar{g}
6 distribution retrieved from the Broadley et al. (2012) data and a surface area correction. A
7 concentration saturation effect appears to be present, whereby the blue, red, and gold
8 experimental data points overlap despite being at different concentrations.

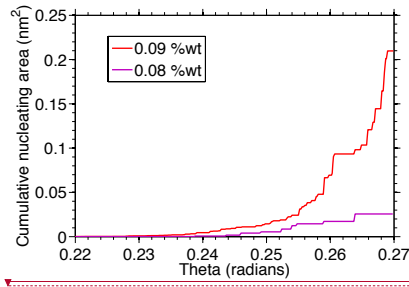
Deleted: 600



12
13
14 **Figure 9.** Cumulative ice nucleating surface areas from application of Eq. (11) to
15 modeled average g distributions from systems 6a (red) and 5a (purple) in Fig. 5, taken
16 from cold plate measurements of illite in droplets from Broadley et al. (2012), plotted
17 against the critical contact angle range. At low contact angles the two systems have close
18 total nucleating surface areas. This explains the similar onset of freezing before the
19 eventual divergence at lower temperature (larger contact angle).



Deleted:



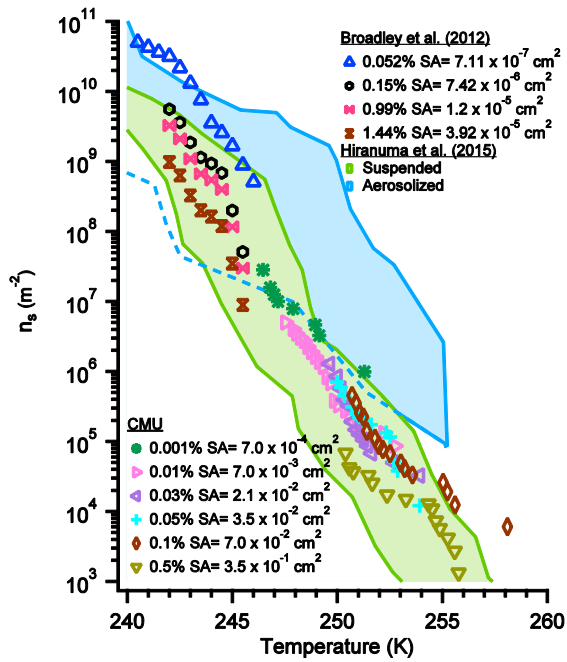
Deleted: [2]

1
2
3
4
5
6
7
8
9
10
11
12

Figure 10. Cumulative ice nucleating surface areas from application of Eq. (11) to modeled average g distributions from droplets containing 0.09 wt% Snomax (red) and 0.08 wt% Snomax (purple) in Fig. 8 plotted against the critical contact angle range. This system does not exhibit similar nucleating areas at low contact angles, and thus does not show an increase in n_s with decreasing concentration (or surface area).

Deleted: green

Deleted: .



1
2
3 **Figure 11.** Range of n_s values for illite NX mineral dust compiled from seventeen
4 measurement methods used by different research groups, the details of which are
5 described by Hiranuma et al. (2015). The range of data is summarized into shaded
6 sections to separate suspended droplet techniques (such as the cold plate) from techniques
7 where the material under investigation is aerosolized before immersion freezing analysis.
8 Data from both the Broadley et al. (2012) and the CMU cold plate systems are also
9 plotted to show how much of the range can be spanned via the critical area effect (blue
10 triangles) and the concentration saturation effect (purple hexagons and red and brown
11 bow ties).

Deleted: ... [3]

